

# **Inhibition of Endothelial Notch Signaling Impairs Fatty Acid Transport and Leads to Metabolic and Vascular Remodeling of the Adult Heart**

**Running Title:** *Jabs et al.; Heart failure After Endothelial Notch Inhibition*

Markus Jabs, PhD, et al.

*The full author list is available on page 19.*

**Address for Correspondence:**

Andreas Fischer, MD  
German Cancer Research Center  
Vascular Signaling and Cancer (A270)  
Im Neuenheimer Feld 280  
69210 Heidelberg, Germany  
Tel: +49 6221 42 4150  
Fax: +49 6221 42 4159  
Email: a.fischer@dkfz.de



Circulation

## Abstract

**Background**—Nutrients are transported through endothelial cells before being metabolized in muscle cells. However, little is known about the regulation of endothelial transport processes. Notch signaling is a critical regulator of metabolism and angiogenesis during development. Here, we studied how genetic and pharmacological manipulation of endothelial Notch signaling in adult mice affects endothelial fatty acid transport, cardiac angiogenesis, and heart function.

**Methods**—Endothelial-specific Notch inhibition was achieved by conditional genetic inactivation of Rbp-jk in adult mice to analyze fatty acid metabolism and heart function. Wild-type mice were treated with neutralizing antibodies against the Notch ligand Dll4. Fatty acid transport was studied in cultured endothelial cells and transgenic mice.

**Results**—Treatment of wild-type mice with Dll4 neutralizing antibodies for eight weeks impaired fractional shortening and ejection fraction in the majority of mice. Inhibition of Notch signaling specifically in the endothelium of adult mice by genetic ablation of Rbp-jk caused heart hypertrophy and failure. Impaired heart function was preceded by alterations in fatty acid metabolism and an increase in cardiac blood vessel density. Endothelial Notch signaling controlled the expression of endothelial lipase, Angptl4, CD36 and Fabp4, which are all needed for fatty acid transport across the vessel wall. In endothelial-specific Rbp-jk-mutant mice lipase activity and transendothelial transport of long-chain fatty acids to muscle cells was impaired. In turn, there was accumulation of lipids in plasma and liver. The attenuated supply of cardiomyocytes with long-chain fatty acids was accompanied by higher glucose uptake, increased concentration of glycolysis intermediates and mTOR-S6K signaling. Treatment with the mTOR inhibitor rapamycin or displacing glucose as cardiac substrate by feeding a ketogenic diet prolonged survival of endothelial-specific Rbp-jk-deficient mice.

**Conclusions**—This study identifies Notch signaling as a novel regulator of fatty acid transport across the endothelium and as an essential repressor of angiogenesis in the adult heart. The data imply that the endothelium controls cardiomyocyte metabolism and function.

**Key Words:** endothelial cell; animal model cardiovascular disease; angiogenesis; metabolism

## Clinical Perspective

### What is new?

- This work shows that Notch signaling in the endothelium controls blood vessel formation and fatty acid transport in the adult mouse heart.
- Inhibition of Notch signaling in the vasculature leads to expansion of the cardiac vasculature and impairment of fatty acid transport to cardiomyocytes.
- This results in metabolic reprogramming and heart failure.

### What are clinical implications?

- Notch signaling is a promising target in oncology.
- Pharmacological inhibition of Notch signaling could lead to heart failure due to vascular and metabolic remodeling of the heart.



# Circulation

## Introduction

Endothelial cells (EC) form tubes for the transport of blood, but in addition, ECs regulate organogenesis, tissue regeneration, stem cell differentiation, or tumor progression in a paracrine (angiocrine) fashion.<sup>1, 2</sup> Given that ECs are in close proximity to almost every other cell type, they are ideally suited to control homeostasis. Even though this may also be important for controlling distribution of nutrients to parenchymal cells, little is known about this.

Located at the interface between plasma and parenchymal cells, EC heterogeneity provides organ-specific vascular beds.<sup>1</sup> For instance, sinusoidal liver ECs form gaps and do not provide a physical barrier for nutrient transport, whereas the continuous endothelium, in muscle, heart, lung or brain requires transcellular transport of nutrients. EC fatty acid transport is facilitated by PPAR $\gamma$  and Meox2/Tcf15,<sup>3, 4</sup> and it is discussed how VEGF-B secreted from cardiomyocytes stimulates EC fatty acid transport.<sup>5-7</sup>

The activity of Notch signaling in various cell types including ECs is influenced by levels of plasma glucose<sup>8-11</sup> and inflammatory lipids,<sup>12</sup> suggesting a link between the metabolic status and Notch signaling activity. Notch signaling is an intercellular communication system. Binding of ligands (Delta-like (Dll) and Jagged) triggers cleavage of Notch receptors to release the intracellular domain (Notch-ICD) that enters the nucleus, interacts with Mastermind like-1 (MAML1) and the Rbp-j $\kappa$  complex to act as a transcription factor. In the developing vasculature and in solid tumors, Dll4/Notch signaling restrains angiogenesis,<sup>13</sup> while in the adult, quiescent endothelium the role of Notch signaling is not yet understood.

Notch signaling is an interesting target for therapeutic interventions in oncology. However, severe congestive heart failure occurred in a substantial proportion of patients treated

with different DLL4-blocking antibodies in phase-I studies,<sup>14, 15</sup> that target Notch signaling predominantly in ECs and a few other cell types. The reason for this remains elusive.

## Methods

The authors declare that all supporting data are available within the article and its online supplementary files.

Please refer to the Expanded Methods in the Online Data Supplements for experimental details.

## Animal Studies

The study was approved by Institutional and Regional Animal Research Committees. All animal procedures were in accordance with institutional guidelines and performed according to the guidelines of the local institution and the local government (Regierungspräsidium Karlsruhe).

*Rbpj*<sup>ΔEC</sup> mice (Cdh5-CreERT2,*Rbpj*<sup>lox/lox</sup>) were obtained by crossing Cdh5-CreERT2 mice with *Rbpj*<sup>lox/lox</sup> mice,<sup>16</sup> and injected with 1.5 mg tamoxifen i.p. for 5 consecutive days. TAG, total ketone bodies and NEFA were measured using kits from Sigma and Wako Diagnostics. Glucose-6-phosphate was determined with a kit from Cayman Chemical Company. Acyl-CoAs were extracted from tissues and measured as described.<sup>17, 18</sup> Mice were not anesthetized during transthoracic echocardiography.<sup>19</sup> Long-chain FA organ uptake was assessed as described.<sup>20</sup> DLL4 blocking antibodies were from Genentech.<sup>21</sup>

## Statistical Analysis

The results are presented as mean and SEM. SigmaPlot 12.5 (Systat Software) was used for statistical analysis. Unpaired two-tailed Student's t-test was used for comparisons of two groups (most of the presented experiments). Significance between more than two groups was tested by

Two Way ANOVA using Holm-Sidak method as post-hoc test. The log-rank test was used to compare survival of mouse cohorts (Fig. 8B).  $p < 0.05$  was considered as statistically significant.

## Results

### Neutralizing DLL4 antibodies impair heart function in mice

Notch1 is expressed in variable amounts in ECs and several other cell types.<sup>22</sup> We observed Notch1 expression in ECs of heart, skeletal muscle, liver and white adipose tissue of adult mice (**Fig. 1A**). In the heart of wild-type mice, there was in particular Notch1 activity in blood vessels as demonstrated by the presence of Notch1-ICD (**Fig. 1B**). Pharmacological targeting of Notch signaling specifically in ECs is not possible up to date. However, expression of the Notch ligand Dll4 is more restricted to the vasculature making this an attractive target to inhibit vascular Notch signaling. Inspired by the fact that heart failure was observed in phase-I trials using neutralizing DLL4 antibodies,<sup>14, 15</sup> we aimed at testing if neutralizing antibodies against murine Dll4<sup>23</sup> would impair heart function also in C57BL6 wild-type mice. Eight weeks after the first injection, freshly isolated ECs had lower mRNA expression levels of *Hey1* and *Hey2* indicative of decreased Notch signaling activity (**Fig. 1C**). The mice had no changes in body weight compared to controls as observed before,<sup>23</sup> the heart to body weight ratio was slightly but not significantly increased (**Fig. 1D**). Transthoracic echocardiography revealed that anti-Dll4 treatment led to a reduction in ejection fraction and fractional shortening in 3 of 5 mice (**Fig. 1E-I**).

### EC-specific Rbp-jk ablation impairs heart function

To test if indeed the inhibition of Notch signaling selectively in the endothelium contributes to development of heart failure, we inactivated the *Rbpj* gene encoding Rbp-jk, the essential

transducer downstream of all four Notch receptors, specifically in ECs.<sup>16</sup> Tamoxifen-driven genetic deletion of *Rbpj* in adult *Cdh5-CreERT2,Rbpj<sup>lox/lox</sup>* mice (*Rbpj<sup>ΔEC</sup>* mice) resulted in robust reduction of Rbp- $\gamma$  protein specifically in ECs but not in whole tissue lysates representing multiple cell types (**Supplementary Fig. 1A, B**). Cre-negative tamoxifen-treated littermates were used as controls. In addition, the cardiac phenotype was also analyzed in Cre-positive tamoxifen-treated mice lacking the floxed allele. As reported before,<sup>23</sup> both controls showed no significant differences.

Heart morphology and weight, as well as cardiac pump function were not altered 4-5 weeks post injection of tamoxifen (p.i.) that leads to endothelial *Rbpj* gene ablation (**Supplementary Fig. 1C-K**). At 6-7 weeks p.i., there was a decrease in ejection fraction (27% vs. 63%,  $p=0.022$ ). Surface electrocardiogram showed no obvious alterations compared to control mice (**Supplementary Fig. S1L**). At 8-10 weeks p.i. the mice died.

Histopathological examination of hearts from *Rbpj<sup>ΔEC</sup>* mice eight weeks p.i. revealed marked hypertrophy of cardiomyocytes, which exhibited larger variance in nuclear size and more cytoplasm, as well as thickening of the left ventricular wall and the septum (**Fig. 2A, B and Supplementary Fig. 2A**). There were no signs of fibrosis (**Supplementary Fig. 2B**), hyperplasia, necrosis or apoptosis. Electron microscopy showed normal arrangement of the cardiac muscle fibers, intercalated discs and normal morphology and localization of mitochondria. However, the mitochondrial size was increased and the mitochondria often contained electron-dense particles likely representing calcium precipitates (**Fig. 2C and Supplementary Fig. 2C, D**), which can form as result of high cytoplasmic calcium levels.<sup>24</sup> Cardiac calcium handling can be impaired due to diminished ATP,<sup>25</sup> and indeed there was a significant reduction of ATP levels in heart lysates of *Rbpj<sup>ΔEC</sup>* mice (**Fig. 2D**). The heart-to-

body-weight ratio was >70% higher in *Rbpj*<sup>iΔEC</sup> than in control animals (**Fig. 2E**).

Echocardiography revealed that the left ventricle was massively enlarged and had an ejection fraction of <20% (**Fig. 2F–I, Supplementary Fig. 2E–H, Supplementary Movie**). The lungs of *Rbpj*<sup>iΔEC</sup> mice were significantly heavier than controls (**Fig. 2E**), indicating pulmonary edema due to reduced pumping function of the left ventricle. This was accompanied by increased expression of the natriuretic peptide *Bnp* (**Fig. 2J**).

Heart failure often leads to a switch in gene expression from the adult towards the “fetal gene expression program”. The fetal heart has a strong preference to carbohydrates over fatty acids as substrates for energy provision and shows lower expression of genes associated with fatty acid oxidation.<sup>26</sup> We detected clear evidence for induction of the fetal gene expression program in hearts of *Rbpj*<sup>iΔEC</sup> mice eight weeks p.i. with altered expression of *glucose transporter-4 (Glut4)*, *pyruvate dehydrogenase isoform-2 (Pdk2)*, *acyl-CoA dehydrogenase, long chain and medium chain (Acadl, Acadm)*, *citrate synthase (Cs)*, *carnitine palmitoyltransferase-1b (Cpt1b)*, *collagen type IIIα (Col3a)* and *myosin heavy polypeptide-6 (Myh6)* (**Fig. 2J**).

### **EC-specific Rbp-jk ablation leads to increased cardiac blood vessel density**

EC Notch signaling restrains angiogenesis during development, ischemia, tissue repair and tumor growth.<sup>13</sup> To test if Notch inhibition would also lead to increased blood vessel growth during heart hypertrophy and failure, blood vessel density was determined. There was already a pronounced alteration in cardiac blood vessel morphology in several spots throughout both ventricles of *Rbpj*<sup>iΔEC</sup> mice at four weeks p.i. and the CD31-positive area was increased compared to controls (**Fig. 3A, B**). Even, in the hypertrophic hearts seven weeks p.i. there was still a very substantial increase in the CD31-positive area. In skeletal muscle, vessel density was

increased at eight weeks p.i., whereas in brain no such changes were observed (**Fig. 3A,C,D**).

The increased cardiac vessel density was associated with higher *CD31* and *Vegfr2* mRNA levels in heart lysates, whereas *Vegf-a* levels, indicative of hypoxia, were not increased (**Fig. 3G**).

To test if these vascular alterations would severely alter blood perfusion we first analyzed skin perfusion and detected no significant changes (**Fig. 3F**). Secondly, Hoechst dye-33342 was injected i.v. and mice sacrificed 60 seconds later. The dye reached essentially all cell nuclei of cardiac muscle in *Rbpj*<sup>iΔEC</sup> (8 weeks p.i.) and control mice, indicating no major defect in blood perfusion (**Fig. 3G**). The same was observed in skeletal muscle (not shown).

### **Elevated plasma TAG and NEFA levels in *Rbpj*<sup>iΔEC</sup> mice**

As the observed vascular alterations appeared unlikely as the sole cause of heart failure, we searched for additional means by which altered EC function could contribute to deterioration of heart function. Changes in cardiac metabolism might cause heart failure.<sup>27</sup> ECs play an important role in shuttling fatty acids to subendothelial cells,<sup>3,4</sup> and could thereby lead to metabolic remodeling in case nutrient transport is impaired. Since the activity of Notch signaling is influenced by several metabolites,<sup>8-12</sup> we aimed at analyzing if EC Notch signaling could be involved in controlling the metabolite flux from plasma to muscle cells.

*Rbpj*<sup>iΔEC</sup> mice showed no differences in body fat and lean masses compared to Cre-negative littermate controls eight weeks p.i. (**Supplementary Fig. 2I**). The morphology of Langerhans islets (**Fig. 4A**) and storage of carbohydrates in liver were comparable to controls (not shown). However, plasma of *Rbpj*<sup>iΔEC</sup> mice showed elevated levels of triacylglycerols (TAG) and non-esterified fatty acids (NEFA, **Fig. 4B,C**) and mice developed fatty liver (**Fig. 4D**). This could be observed already at 3-4 weeks p.i., when cardiac output function was still

normal. This indicated that EC Notch signaling might be needed for the transendothelial transport of fatty acids.

### **EC Notch signaling is needed for clearance of plasma TAG**

TAG are processed into fatty acids by lipases apically bound to ECs. It is important to note that the discontinuous liver endothelium is no barrier for fatty acid uptake by hepatocytes. In turn, the continuous endothelium in muscle provides transcellular transport of fatty acids.<sup>1</sup>

First we analyzed a potential crosstalk between the endothelium and fatty acid metabolism in liver. Liver histology showed regular trabecular architecture. Fibrosis, necrosis or overt inflammation were not present (**Fig. 4A**). The expression of genes involved in lipogenesis in liver lysates of *Rbpj*<sup>iΔEC</sup> mice did not indicate increased hepatic TAG production neither was the expression of beta-oxidation enzymes altered (**Fig. 4E,F**). Furthermore, blockade of vascular lipolysis by tyloxapol, showed that hepatic TAG production was not increased in *Rbpj*<sup>iΔEC</sup> mice compared to controls (**Fig. 4G**). As hepatic lipid metabolism unlikely explained the accumulation of TAG in liver and plasma, we hypothesized that transendothelial fatty acid transport in organs containing a continuous endothelium could be impaired.

To test this, we first challenged *Rbpj*<sup>iΔEC</sup> mice (4-5 weeks p.i.) with oral application of olive oil. As expected, plasma TAG levels first increased to a maximum, which was similar in both genotypes. Then the circulatory TAG levels of *Rbpj*<sup>iΔEC</sup> mice decreased more slowly than those of controls, suggesting lower TAG clearance into the tissues as indicated by a smaller slope between peak and end of the experiment (**Fig. 4H,I**). Importantly, fat resorption from the gut did not seem to be impaired as defecation rate as well as TAG concentration in feces were similar in both genotypes (**Fig. 4J,K**).

### EC Notch signaling is required for vascular lipolysis and transport of NEFAs

The TAG clearance test indicated that loss of EC Notch signaling either leads to decreased lipase activity or to reduced EC transcytosis of fatty acids. Indeed, we detected a  $\approx 50\%$  reduction of plasma lipase activity in *Rbpj* <sup>$\Delta$ EC</sup> mice (**Fig. 5A**). Secondly we analyzed if not only lipase activity but also the transendothelial fatty acid transport would be controlled by Notch signaling. To this end, the uptake of intravenously injected tracer <sup>3</sup>H-R-bromopalmitate, a slowly metabolized palmitate analogue, into different organs was measured. Compared to controls, *Rbpj* <sup>$\Delta$ EC</sup> mice (five weeks p.i.) had lower uptake rates of palmitate into heart and skeletal muscle. As expected no alterations were seen in liver (**Fig. 5B, C**), in which the sinusoidal endothelium does not act as a tight barrier.



Based on these experiments, we expected to detect diminished levels of activated fatty acids (acyl-CoA) in cardiac and skeletal muscle of *Rbpj* <sup>$\Delta$ EC</sup> mice. Indeed, acyl-CoA levels were reduced to 80% in skeletal muscle and to 55% in hearts of *Rbpj* <sup>$\Delta$ EC</sup> mice compared to controls (**Fig. 5D**). Detailed analysis of fatty acids bound to carnitine revealed that there was a decrease in long-chain, but not medium-chain or short-chain fatty acids in cardiac muscle (**Fig. 5E**).

### Notch signaling facilitates uptake of fatty acids into cultured ECs

Next, we aimed at analyzing the transport of fatty acids into ECs in an *in vitro* setting to exclude potential effects of unknown factors that may interfere with such transport in transgenic mouse models. We first tested whether Notch signaling generally alters paracellular flux through an EC monolayer *in vitro*, because this would affect monitoring the specific transport of fatty acids. Therefore we manipulated Notch signaling activity in primary human umbilical venous ECs (HUVEC), the prototypic tool for EC research.

Notch inhibition increased paracellular permeability as determined by measuring transendothelial electrical resistance and capacity (**Supplementary Fig. 3A**). Also the flux of fluorescent 4 kDa dextran tracers in a transwell filter assay was increased after Notch inhibition, whereas no such changes were observed with 40 kDa dextran tracers (**Supplementary Fig. 3B, C**), indicating a size-selective opening of paracellular transport routes.

*In vivo*, extravasation of Evans blue (bound to plasma proteins) was however not increased in *Rbpj*<sup>ΔEC</sup> mice compared to littermate controls both under basal conditions or after stimulation with histamine. In the latter, there was even a slight reduction of paracellular permeability compared to control animals (**Supplementary Fig. 3D**). Likewise in a peritonitis assay, *Rbpj*<sup>ΔEC</sup> mice exhibited no signs of increased permeability compared to controls (**Supplementary Fig. 3E, F**). Also basal paracellular permeability of 10 kDa and 40 kDa tracers was similar in hearts of *Rbpj*<sup>ΔEC</sup> mice compared to controls (**Supplementary Fig. 3G, H**).

Hence, inhibition of Notch signaling promotes paracellular flux of small molecules *in vitro* but not *in vivo*. For this reason we could not determine how Notch inhibition alters the transport of fatty acids through an EC monolayer *in vitro*. However we could detect that inhibition of Notch signaling impaired the uptake of a fluorescent palmitate analogue into HUVEC, whereas this was increased upon Notch stimulation by recombinant DLL4 (**Fig. 5F**).

#### **Notch controls expression of *LIPG* and *ANGPTL4* to facilitate vascular lipolysis**

Next, we aimed at identifying mechanisms how EC Notch signaling controls fatty acids transport. Notch/Rbp- $\text{j}\kappa$  signaling activate gene expression by binding to promoter elements or represses gene expression indirectly by induction of HES and HEY transcriptional repressors. The activity of Notch signaling was inhibited by expression of dnMAML1 and enhanced by expression of Notch1-ICD in HUVEC and efficiency was controlled by qPCR assessing target

genes (*HEY1*, *HEY2*, *DLL4*, *EFNB2*). Notch inhibition led to decreased transcription of *endothelial lipase (LIPG)* (**Fig. 6A**), which hydrolyses mainly phospholipids but also TAG.

In addition to hydrolysis by LIPG, fatty acids can also be released from TAG-containing lipoproteins by lipoprotein lipase. This lipase is synthesized and secreted by parenchymal cells (e.g. cardiomyocytes) and subsequently bound at the apical EC surface by *Gpihbp1*.<sup>28, 29</sup> Expression of *Gpihbp1* in primary cardiac ECs isolated from *Rbpj*<sup>ΔEC</sup> mice was similar to expression in cells isolated from controls (**Fig. 6B**).

Vascular lipolysis is also controlled by the non-competitive lipoprotein lipase inhibitor *angiopoietin-like 4 (ANGPTL4)*. Notch inhibition in HUVEC led to increased expression of *ANGPTL4* mRNA, whereas Notch1-ICD decreased it (**Fig. 6A**). ECs isolated from hearts or lungs of *Rbpj*<sup>ΔEC</sup> mice had increased expression levels of *Angptl4* mRNA (**Fig. 6C**). Notch blockade in HUVEC increased ANGPTL4 protein amounts (**Fig. 6D**). Consistently, hearts from *Rbpj*<sup>ΔEC</sup> mice contained substantially more *Angptl4* protein-expressing ECs compared to controls as indicated by a stronger colocalization with lectin-GS-IB4 (**Supplementary Fig. S4**), indicating that EC Notch signaling inhibits production of the lipoprotein lipase inhibitor *Angptl4*.

### **EC Notch signaling induces *CD36* and *FABP4/5* to facilitate fatty acid transport**

After lipolysis, fatty acid transport proteins (in particular *Fatp4*) take up fatty acids into ECs. Uptake of long-chain fatty acids is supported by *fatty acid translocase (CD36)*. While the mRNA expression of *Fatp4* and of *acyl-CoA synthetases* was not altered we detected lower levels of *CD36* expression upon Notch inhibition and higher *CD36* mRNA levels in cells with increased Notch activity (**Fig. 6A**). In freshly isolated cardiac and lung ECs from *Rbpj*<sup>ΔEC</sup> mice lower *CD36* mRNA expression was observed (**Fig. 6C**), and protein regulation could be verified in

primary cardiac ECs (**Fig. 6E**). In cultured ECs, CD36 expression increased the uptake of fluorescently palmitate (**Fig. 6F**) as reported before.<sup>30</sup>

Notch signaling induces the expression of *fatty acid binding protein 4 (FABP4)*, an intracellular lipid chaperone, by binding of Rbp-j $\kappa$  to the *FABP4* promoter.<sup>31</sup> We confirmed this gene regulation and found that Notch1-ICD also induces *FABP5* in HUVECs. Consistently, HUVECs expressing dnMAML1 had reduced expression of *FABP4* (**Fig. 6A,G**).

EC fatty acid transport is facilitated by PPAR $\gamma$  that stimulates expression of *CD36* and *FABP4*.<sup>4</sup> However, treatment of EC with the PPAR $\gamma$  inhibitor T0070907 did not prevent the effect of Notch1-ICD on the expression of *CD36*, *FABP4* and *ANGPTL4* (**Fig. 6H**). Chromatin immunoprecipitation revealed that Rbp-j $\kappa$  interacts with a *CD36* promoter element, which contains two putative Rbp-j $\kappa$ -binding sites (TG[G/A]GAA) (**Fig. 6I**). Taken together, inhibition of Notch signaling led to decreased expression of *LIPG*, *CD36*, and *FABP4*, while transcription of the lipoprotein lipase inhibitor *ANGPTL4* increased, indicating that EC Notch signaling is essential for proper TAG hydrolysis and long-chain fatty acid transport.

### **EC-specific Rbp-j $\kappa$ ablation changes cardiac nutrient supply leading to accumulation of monosaccharides and their metabolites**

The heart oxidizes long-chain fatty acids to generate the majority of its energy need.<sup>32</sup> An imbalance of fatty acid and glucose supply has been proposed as a potential cause of cardiac remodeling and failure.<sup>26,27</sup>

We had observed a 2-fold reduction of activated fatty acids in heart lysates of *Rbpj*<sup>i $\Delta$ EC</sup> mice (**Fig. 5D**), and expected a compensatory increase in glucose uptake and consumption. Indeed, positron emission tomography revealed that cardiac uptake of <sup>18</sup>F-fluoro-2-deoxy-D-glucose was substantially increased in *Rbpj*<sup>i $\Delta$ EC</sup> mice (**Fig. 7A,B**). This increase is in a similar

magnitude as observed in a different mouse model, which develops impaired cardiac contractility due to decreased endothelial fatty acid transport.<sup>3</sup> The elevated glucose uptake was accompanied by 3-fold higher levels of glucose-6-phosphate in hearts of *Rbpj*<sup>iΔEC</sup> mice (5-6 weeks p.i.) (**Fig. 7C**). In addition to accumulation of glucose-6-phosphate, we detected a marked increase in glucose, maltose, sucrose and mannose, all of which can be derived from glucose, in hearts of *Rbpj*<sup>iΔEC</sup> mice, while plasma glucose levels were decreased compared to controls (**Fig. 7D,E**). PAS staining did not show signs of glycogen accumulation in hearts six weeks p.i. (data not shown). However, there were higher levels of pyruvate in *Rbpj*<sup>iΔEC</sup> hearts (**Fig. 7F**). These data sets suggested that there was a shift in nutrient supply to the heart muscle with increased glucose uptake to compensate the impaired fatty acid transport.



### **Cardiac accumulation of glucose-6-phosphate is accompanied by sustained AKT and mTOR-S6K signaling**

It is assumed that sustained accumulation of glucose-derived metabolites and increased glycolysis rates activate mTOR-S6K signaling and other pathways leading to cell hypertrophy and subsequent heart failure.<sup>26, 33-38</sup> Therefore, we analyzed the activity of kinases that are involved in cardiac hypertrophy in heart lysates. The phosphorylation of AKT, ERK1/2, mTOR, p70S6K, and S6 was significantly enhanced in *Rbpj*<sup>iΔEC</sup> mice seven weeks p.i. (**Fig. 8A, Supplementary Fig. 5A**).

To test how glucose or its metabolites act on S6K activation, freshly isolated neonatal rat cardiomyocytes were treated with 5 g/L glucose. This led to robust induction of S6K activity. 3-O-methyl-glucose alone, which is taken up by cells but is not phosphorylated and metabolized, did not activate S6K and did not prevent glucose-induced S6K activation. However, 2-deoxy-

glucose, an inhibitor of glycolysis, prevented glucose-mediated induction of S6K activity (**Supplementary Fig. S5B**).

### **Interventional therapy with rapamycin or feeding a ketogenic diet prolongs survival of *Rbpj*<sup>ΔEC</sup> mice**

*Rbpj*<sup>ΔEC</sup> mice developed severely impaired heart function around 8-10 weeks p.i., which was associated with increased mTOR-S6K activity. Rapamycin inhibits mTOR signaling and prevents mTOR-mediated cardiac hypertrophy and heart failure in rodent models.<sup>37,38</sup> We treated *Rbpj*<sup>ΔEC</sup> mice with rapamycin (2 mg/kg i.p. every day) in the time period 8-11 weeks after gene recombination. While sham-treated *Rbpj*<sup>ΔEC</sup> mice died in this period, rapamycin-treated mice had a strongly increased survival rate (p=0.02) (**Fig. 8B**).



Since rapamycin has a strong immunosuppressive effect, we searched also for alternative treatments. We propose that the impairment of heart function in *Rbpj*<sup>ΔEC</sup> mice occurs to a large extent due to a shift from long-chain fatty acid to carbohydrate supply to cardiomyocytes. Therefore, one could potentially interfere by restricting the availability of glucose to a minimum and to increase supply of alternative substrates for mitochondrial oxidation, which do not require EC lipase activity and transport via CD36 and Fabp4/5 and which do not activate mTOR signaling. A strict ketogenic diet is ideally suited to fulfill these requirements. Amino acids from dietary protein are the source to generate glucose for nourishing erythrocytes and neurons, while fat is converted by hepatocytes into ketone bodies, a preferred energy substrate for cardiomyocytes. In addition, cardiac utilization of ketone bodies inhibits oxidation of fat and glucose.<sup>34</sup> Notably, ketone bodies are transported by monocarboxylate transporters, whose expression was not severely affected by loss of Rbp-jκ (**Supplementary Fig. 5C**).

First, *Rbpj*<sup>iΔEC</sup> mice were fed with a ketogenic diet (0.2% carbohydrates, 67% fat, 18% proteins per weight) in the time period 8-11 weeks p.i., which raised levels of total plasma ketone bodies by more than 5-fold ( $p < 0.01$ ). Compared to *Rbpj*<sup>iΔEC</sup> mice fed with a control diet (67% carbohydrates, 4% fat, 19% proteins per weight), the *Rbpj*<sup>iΔEC</sup> mice fed with a ketogenic diet survived significantly longer ( $p = 0.03$ ) (**Fig. 8B**). Based on this, mice were fed with a ketogenic diet starting immediately after gene recombination. Eight weeks later, echocardiography showed that *Rbpj*<sup>iΔEC</sup> mice fed with a ketogenic diet had similar heart function as Cre-negative control animals, whereas *Rbpj*<sup>iΔEC</sup> mice fed with a control diet suffered from severe heart failure (**Fig. 8C - G and Supplementary Fig. 5D - H**). The degree of impairment observed in the control-fed *Rbpj*<sup>iΔEC</sup> mice was less pronounced as reported in **Figure 2**. The reason for this is likely the slightly variable onset of the phenotype and that in the night before the examination three control-fed *Rbpj*<sup>iΔEC</sup> mice died (who had severely enlarged hearts). Consistently with the improvement of cardiac function, the levels of glucose-6-phosphate were lower in *Rbpj*<sup>iΔEC</sup> mice fed with ketogenic diet compared to those fed with control diet (**Fig. 8H**).

## Discussion

This study has revealed critical and rate-limiting functions of EC Notch signaling in adult mice as a novel regulator of cardiac blood vessel growth and fatty acid transport across the vessel wall. Notch signaling controls numerous cell fate differentiation steps during development, tissue regeneration and repair. Little is known about its roles for maintenance of homeostasis in the adult organism. Recently, it was shown that elevated Notch activity promotes hepatic glucose production and reduces browning of adipose tissue, while genetic ablation of Rbp-jk in hepatocytes or adipose cells as well as global Notch1 deficiency improved insulin sensitivity.<sup>8, 11,</sup>

<sup>39</sup> Since the metabolic status influences Notch signaling activity not only in hepatocytes but also other cell types including ECs,<sup>8-12</sup> we analyzed the roles of Notch in the adult endothelium of mice with an emphasis on metabolism. The data show that Notch signals in the endothelium are needed for proper transcriptional control of key genes (*Lipg*, *Angptl4*, *CD36*, *Fabp4/5*) for TAG hydrolysis and long-chain fatty acid transport through ECs. EC-specific targeting of Rbp-jk led to impaired hydrolysis of TAG and decreased transport of long-chain fatty acids to heart muscle. This was associated with a switch from fatty acids to glucose as sources for energy production. Such a switch is also well known from several animal models of heart failure. Increased amounts of glycolysis intermediates can activate AKT and mTOR-S6K signaling. Sustained activity of these signaling pathways in cardiomyocytes induces cardiac hypertrophy followed by heart failure.<sup>35, 36</sup>

Secondly, this work demonstrates an essential role of Rbp-jk for inhibiting blood vessel growth in the adult heart. Notch and Rbp-jk inhibition during the embryo-fetal and perinatal period leads to increased sprouting angiogenesis and defects in arterio-venous differentiation.<sup>13, 40, 41</sup> Dll4 neutralizing antibodies can induce the formation of vascular tumor-like structures upon long-term treatment.<sup>42</sup> Here we show that blood vessel density was increased upon deletion of Rbp-jk in the heart. We hypothesize that any form of tissue growth (e.g. cardiac hypertrophy) or tissue remodeling will result in aberrant and blood vessel growth in case Notch signaling is inhibited. It will be fascinating to decipher this in detail in future studies.

At this stage, one cannot definitely decide if heart failure occurs solely due to impaired fatty acid transport in *Rbpj*<sup>iΔEC</sup> mice. Although perfusion studies did not show obvious defects one can assume – based on studies in tumors<sup>21</sup> – that the remodeled cardiac vasculature is not fully functional. Nevertheless, several other observations strengthen the hypothesis that altered

nutrient supply to cardiomyocytes upon EC-specific deletion of Rbp-jk is important for deterioration of heart function. We detected increased expression of *Angptl4*, a secreted non-competitive inhibitor of lipoprotein lipase,<sup>43</sup> in ECs isolated from *Rbpj<sup>iΔEC</sup>* mice. Cardiac-specific overexpression of *Angptl4* causes heart failure in mice.<sup>44</sup> *Lipg* expression was impaired in *Rbpj<sup>iΔEC</sup>* mice. Mice deficient for this endothelial lipase are viable, but heart function is stronger impaired after aortic banding compared to controls.<sup>45</sup> Additionally, global deficiency for *Fabp4/Fabp5* causes cardiac metabolic remodeling and mild heart hypertrophy in mice, which was attributed to the lack of these proteins in cardiac endothelium.<sup>46</sup> The phenotype of *Rbpj<sup>iΔEC</sup>* mice is more severe, but one should notice that in these animals there is miss-regulation of a whole set of genes controlling or executing different steps of fatty acid hydrolysis and transport together with alterations in vascular patterning. Lastly, our interventional experiments with rapamycin and ketogenic diet further strengthened the importance of metabolic remodeling as an important cause of worsened heart function in *Rbpj<sup>iΔEC</sup>* mice. In summary, this work demonstrates the importance of angiocrine functions for maintenance of cardiac homeostasis.

## Authors

Markus Jabs, PhD<sup>1</sup>; Adam J. Rose, PhD<sup>2</sup>; Lorenz H. Lehmann, MD<sup>3,4</sup>;  
 Jacqueline Taylor, MSc<sup>1</sup>; Iris Moll, MLS<sup>1</sup>; Tjeerd P. Sijmonsma, BcS<sup>2</sup>;  
 Stefanie E. Herberich, PhD<sup>1</sup>; Sven W. Sauer, PhD<sup>5</sup>; Gernot Poschet, PhD<sup>6</sup>;  
 Giuseppina Federico, PhD<sup>7</sup>; Carolin Mogler, MD<sup>8</sup>; Eva-Maria Weis, MSc<sup>1</sup>;  
 Hellmut G. Augustin, DVM, PhD<sup>9,10</sup>; Minhong Yan, PhD<sup>11</sup>; Norbert Gretz, MD<sup>12</sup>;  
 Roland M. Schmid, MD<sup>13</sup>; Ralf H. Adams, PhD<sup>14</sup>; Hermann-Joseph Gröne, MD<sup>7</sup>;  
 Rüdiger Hell, PhD<sup>6</sup>; Jürgen G. Okun, PhD<sup>5</sup>; Johannes Backs, MD<sup>3</sup>; Peter P. Nawroth, MD<sup>15</sup>;

Stephan Herzig, PhD<sup>16</sup>; Andreas Fischer, MD<sup>1,10,15\*</sup>

## Affiliations

<sup>1</sup>Vascular Signaling and Cancer, DKFZ-ZMBH Alliance and German Cancer Research Center (DKFZ), Heidelberg, Germany; <sup>2</sup>Joint Division Molecular Metabolic Control, DKFZ-ZMBH Alliance and Network Aging Research, German Cancer Research Center (DKFZ) Heidelberg, Center for Molecular Biology (ZMBH) and University Hospital Heidelberg University, Heidelberg, Germany & Nutrient Metabolism and Signalling Lab, Dept. Biochemistry & Molecular Biology, Monash Biomedicine Discovery Institute, Monash University, Clayton, VIC, Australia; <sup>3</sup>Department of Molecular Cardiology and Epigenetics, University Hospital of Heidelberg, Heidelberg, Germany & German Centre for Cardiovascular Research (DZHK), Partner Site Heidelberg/Mannheim, Heidelberg, Germany; <sup>4</sup>Department of Cardiology, University Hospital of Heidelberg, Heidelberg, Germany; <sup>5</sup>Department of General Pediatrics, Division of Inherited Metabolic Diseases, University Children's Hospital Heidelberg, Heidelberg, Germany; <sup>6</sup>Centre for Organismal Studies (COS), Heidelberg University, Heidelberg, Germany; <sup>7</sup>Division of Cellular and Molecular Pathology, German Cancer Research Center (DKFZ), Heidelberg, Germany; <sup>8</sup>Institute for Pathology, Technical University of Munich, Munich, Germany; <sup>9</sup>Vascular Oncology and Metastasis, DKFZ-ZMBH Alliance and German Cancer Research Center (DKFZ), Heidelberg, Germany; <sup>10</sup>Vascular Biology (CBTM), Medical Faculty Mannheim, Heidelberg University, Mannheim, Germany; <sup>11</sup>Molecular Oncology, Genentech, Inc., 1 DNA Way, South San Francisco, CA; <sup>12</sup>Medical Research Center, University of Heidelberg, Mannheim, Germany; <sup>13</sup>Department of Medicine II, Klinikum rechts der Isar, Technische Universität München, Munich, Germany; <sup>14</sup>Max Planck Institute for Molecular

Biomedicine, Department of Tissue Morphogenesis and University of Münster, Faculty of Medicine, Münster, Germany; <sup>15</sup>Department of Medicine I and Clinical Chemistry, University Hospital of Heidelberg, Heidelberg, Germany; <sup>16</sup>Institute for Diabetes and Cancer (IDC) and Joint Heidelberg-IDC Translational Diabetes Program, Helmholtz Center Munich, Neuherberg, Germany.

\*Correspondence to: a.fischer@dkfz.de

### **Acknowledgments**

We thank Kerstin Wöltje, Annika Zota and Kathrin Schmidt for technical assistance. We thank the Metabolomics Core Technology Platform of the Excellence Cluster CellNetworks for support with HPLC-based metabolite quantification and the small animal imaging facility at DKFZ and especially Viktoria Eichwald for excellent support with PET scans and data analysis.

### **Sources of Funding**

This work was supported by grants from the German Research Foundation (DFG FI 1569/3-1 to AF; GRK880 to M.J., A.F. and H.G.A.; SFB-TR23 to A.F., H.G.A.; SFB1118 to H.J.G., J.B., P.P.N., S.H.), the Chica and Heinz Schaller foundation to A.F., the Dietmar Hopp Foundation to P.P.N., the European Union's Horizon 2020 research and innovation programme under grant agreement No 692322 to A.F., the Deutsches Zentrum für Herz-Kreislauf-Forschung (German Centre for Cardiovascular Research, DZHK) to J.B. and the German Ministry of Education and Research (BMBF) to J.B.

## Disclosures

Dr. Minhong Yan is a Genentech employee. The other authors have nothing to disclose.

## References

1. Augustin HG, Koh GY. Organotypic vasculature: From descriptive heterogeneity to functional pathophysiology. *Science*. 2017;357. doi:10.1126/science.aal2379.
2. Ramasamy SK, Kusumbe AP, Adams RH. Regulation of tissue morphogenesis by endothelial cell-derived signals. *Trends Cell Biol*. 2015;25:148-157. doi:10.1016/j.tcb.2014.11.007.
3. Coppiello G, Collantes M, Sirerol-Piquer MS, Vandenwijngaert S, Schoors S, Swinnen M, Vandersmissen I, Herijgers P, Topal B, van Loon J, Goffin J, Prosper F, Carmeliet P, Garcia-Verdugo JM, Janssens S, Penuelas I, Aranguren XL, Lutun A. Meox2/Tcf15 heterodimers program the heart capillary endothelium for cardiac fatty acid uptake. *Circulation*. 2015;131:815-826. doi:10.1161/CIRCULATIONAHA.114.013721.
4. Kanda T, Brown JD, Orasanu G, Vogel S, Gonzalez FJ, Sartoretto J, Michel T, Plutzky J. PPARgamma in the endothelium regulates metabolic responses to high-fat diet in mice. *J Clin Invest*. 2009;119:110-124. doi:10.1172/JCI36233.
5. Dijkstra MH, Pirinen E, Huusko J, Kivela R, Schenkwein D, Alitalo K, Yla-Herttuala S. Lack of cardiac and high-fat diet induced metabolic phenotypes in two independent strains of Vegf-b knockout mice. *Sci Rep*. 2014;4:6238. doi:10.1038/srep06238.
6. Hagberg CE, Falkevall A, Wang X, Larsson E, Huusko J, Nilsson I, van Meeteren LA, Samén E, Lu L, Vanwildemeersch M, Klar J, Genove G, Pietras K, Stone-Elander S, Claesson-Welsh L, Yla-Herttuala S, Lindahl P, Eriksson U. Vascular endothelial growth factor B controls endothelial fatty acid uptake. *Nature*. 2010;464:917-921. doi:10.1038/nature08945.
7. Kivela R, Bry M, Robciuc MR, Rasanen M, Taavitsainen M, Silvola JM, Saraste A, Hulmi JJ, Anisimov A, Mayranpaa MI, Lindeman JH, Eklund L, Hellberg S, Hlushchuk R, Zhuang ZW, Simons M, Djonov V, Knuuti J, Mervaala E, Alitalo K. VEGF-B-induced vascular growth leads to metabolic reprogramming and ischemia resistance in the heart. *EMBO Mol Med*. 2014;6:307-321. doi:10.1002/emmm.201303147.
8. Bi P, Shan T, Liu W, Yue F, Yang X, Liang XR, Wang J, Li J, Carlesso N, Liu X, Kuang S. Inhibition of Notch signaling promotes browning of white adipose tissue and ameliorates obesity. *Nat Med*. 2014;20:911-918. doi:10.1038/nm.3615.
9. Gao F, Yao M, Shi Y, Hao J, Ren Y, Liu Q, Wang X, Duan H. Notch pathway is involved in high glucose-induced apoptosis in podocytes via Bcl-2 and p53 pathways. *J Cell Biochem*. 2013;114:1029-1038. doi:10.1002/jcb.24442.
10. Pajvani UB, Qiang L, Kangsamaksin T, Kitajewski J, Ginsberg HN, Accili D. Inhibition of Notch uncouples Akt activation from hepatic lipid accumulation by decreasing mTORc1 stability. *Nat Med*. 2013;19:1054-1060. doi:10.1038/nm.3259.
11. Pajvani UB, Shawber CJ, Samuel VT, Birkenfeld AL, Shulman GI, Kitajewski J, Accili D. Inhibition of Notch signaling ameliorates insulin resistance in a FoxO1-dependent manner. *Nat Med*. 2011;17:961-967. doi:10.1038/nm.2378.
12. Briot A, Civelek M, Seki A, Hoi K, Mack JJ, Lee SD, Kim J, Hong C, Yu J, Fishbein GA, Vakili L, Fogelman AM, Fishbein MC, Lusis AJ, Tontonoz P, Navab M, Berliner JA, Iruela-

- Arispe ML. Endothelial NOTCH1 is suppressed by circulating lipids and antagonizes inflammation during atherosclerosis. *J Exp Med*. 2015;212:2147-2163. doi:10.1084/jem.20150603.
13. Potente M, Gerhardt H, Carmeliet P. Basic and therapeutic aspects of angiogenesis. *Cell*. 2011;146:873-887. doi:10.1016/j.cell.2011.08.039.
  14. Chiorean EG, LoRusso P, Strother RM, Diamond JR, Younger A, Messersmith WA, Adriaens L, Liu L, Kao RJ, DiCioccio AT, Kostic A, Leek R, Harris A, Jimeno A. A Phase I First-in-Human Study of Enoticumab (REGN421), a Fully Human Delta-like Ligand 4 (Dll4) Monoclonal Antibody in Patients with Advanced Solid Tumors. *Clin Cancer Res*. 2015;21:2695-2703. doi:10.1158/1078-0432.CCR-14-2797.
  15. Smith DC, Eisenberg PD, Manikhas G, Chugh R, Gubens MA, Stagg RJ, Kapoun AM, Xu L, Dupont J, Sikic B. A phase I dose escalation and expansion study of the anticancer stem cell agent demcizumab (anti-DLL4) in patients with previously treated solid tumors. *Clin Cancer Res*. 2014;20:6295-6303. doi:10.1158/1078-0432.CCR-14-1373.
  16. Ramasamy SK, Kusumbe AP, Wang L, Adams RH. Endothelial Notch activity promotes angiogenesis and osteogenesis in bone. *Nature*. 2014;507:376-380. doi:10.1038/nature13146.
  17. Barber ED, Lands WE. Determination of acyl-CoA concentrations using pancreatic lipase. *Biochim Biophys Acta*. 1971;250:361-366.
  18. Golovko MY, Murphy EJ. An improved method for tissue long-chain acyl-CoA extraction and analysis. *J Lipid Res*. 2004;45:1777-1782. doi:10.1194/jlr.D400004-JLR200.
  19. Lehmann LH, Rostovsky JS, Buss SJ, Kreusser MM, Krebs J, Mier W, Enseleit F, Spiger K, Hardt SE, Wieland T, Haass M, Luscher TF, Schneider MD, Parlato R, Grone HJ, Haberkorn U, Yanagisawa M, Katus HA, Backs J. Essential role of sympathetic endothelin A receptors for adverse cardiac remodeling. *Proc Natl Acad Sci U S A*. 2014;111:13499-13504. doi:10.1073/pnas.1409026111.
  20. Furler SM, Cooney GJ, Hegarty BD, Lim-Fraser MY, Kraegen EW, Oakes ND. Local factors modulate tissue-specific NEFA utilization: assessment in rats using 3H-(R)-2-bromopalmitate. *Diabetes*. 2000;49:1427-1433.
  21. Ridgway J, Zhang G, Wu Y, Stawicki S, Liang WC, Chanthery Y, Kowalski J, Watts RJ, Callahan C, Kasman I, Singh M, Chien M, Tan C, Hongo JA, de Sauvage F, Plowman G, Yan M. Inhibition of Dll4 signalling inhibits tumour growth by deregulating angiogenesis. *Nature*. 2006;444:1083-1087. doi:10.1038/nature05313.
  22. Hofmann JJ, Iruela-Arispe ML. Notch signaling in blood vessels: who is talking to whom about what? *Circ Res*. 2007;100:1556-1568. doi:10.1161/01.RES.0000266408.42939.e4.
  23. Wieland E, Rodriguez-Vita J, Liebler SS, Mogler C, Moll I, Herberich SE, Espinet E, Herpel E, Menuchin A, Chang-Claude J, Hoffmeister M, Gebhardt C, Brenner H, Trumpp A, Siebel CW, Hecker M, Utikal J, Sprinzak D, Fischer A. Endothelial Notch1 Activity Facilitates Metastasis. *Cancer Cell*. 2017;31:355-367. doi:10.1016/j.ccell.2017.01.007.
  24. Szabadkai G, Duchon MR. Mitochondria: the hub of cellular Ca<sup>2+</sup> signaling. *Physiology (Bethesda)*. 2008;23:84-94. doi:10.1152/physiol.00046.2007.
  25. Luo M, Anderson ME. Mechanisms of altered Ca<sup>2+</sup>(+) handling in heart failure. *Circ Res*. 2013;113:690-708. doi:10.1161/CIRCRESAHA.113.301651.
  26. Taegtmeier H, Sen S, Vela D. Return to the fetal gene program: a suggested metabolic link to gene expression in the heart. *Ann N Y Acad Sci*. 2010;1188:191-198. doi:10.1111/j.1749-6632.2009.05100.x.

27. Kundu BK, Zhong M, Sen S, Davogustto G, Keller SR, Taegtmeier H. Remodeling of glucose metabolism precedes pressure overload-induced left ventricular hypertrophy: review of a hypothesis. *Cardiology*. 2015;130:211-220. doi:10.1159/000369782.
28. Davies BS, Beigneux AP, Barnes RH, 2nd, Tu Y, Gin P, Weinstein MM, Nobumori C, Nyren R, Goldberg I, Olivecrona G, Bensadoun A, Young SG, Fong LG. GPIHBP1 is responsible for the entry of lipoprotein lipase into capillaries. *Cell Metab*. 2010;12:42-52. doi:10.1016/j.cmet.2010.04.016.
29. O'Brien KD, Ferguson M, Gordon D, Deeb SS, Chait A. Lipoprotein lipase is produced by cardiac myocytes rather than interstitial cells in human myocardium. *Arterioscler Thromb*. 1994;14:1445-1451.
30. Goto K, Iso T, Hanaoka H, Yamaguchi A, Suga T, Hattori A, Irie Y, Shinagawa Y, Matsui H, Syamsunarno MR, Matsui M, Haque A, Arai M, Kunimoto F, Yokoyama T, Endo K, Gonzalez FJ, Kurabayashi M. Peroxisome proliferator-activated receptor-gamma in capillary endothelia promotes fatty acid uptake by heart during long-term fasting. *J Am Heart Assoc*. 2013;2:e004861. doi:10.1161/JAHA.112.004861.
31. Harjes U, Bridges E, McIntyre A, Fielding BA, Harris AL. Fatty acid-binding protein 4, a point of convergence for angiogenic and metabolic signaling pathways in endothelial cells. *J Biol Chem*. 2014;289:23168-23176. doi:10.1074/jbc.M114.576512.
32. Gallagher D, Belmonte D, Deurenberg P, Wang Z, Krasnow N, Pi-Sunyer FX, Heymsfield SB. Organ-tissue mass measurement allows modeling of REE and metabolically active tissue mass. *Am J Physiol*. 1998;275:E249-258.
33. Buller CL, Heilig CW, Brosius FC, 3rd. GLUT1 enhances mTOR activity independently of TSC2 and AMPK. *Am J Physiol Renal Physiol*. 2011;301:F588-596. doi:10.1152/ajprenal.00472.2010.
34. Kolwicz SC, Jr., Purohit S, Tian R. Cardiac metabolism and its interactions with contraction, growth, and survival of cardiomyocytes. *Circ Res*. 2013;113:603-616. doi:10.1161/CIRCRESAHA.113.302095.
35. Sciarretta S, Volpe M, Sadoshima J. Mammalian target of rapamycin signaling in cardiac physiology and disease. *Circ Res*. 2014;114:549-564. doi:10.1161/CIRCRESAHA.114.302022.
36. Wende AR, O'Neill BT, Bugger H, Riehle C, Tuinei J, Buchanan J, Tsushima K, Wang L, Caro P, Guo A, Sloan C, Kim BJ, Wang X, Pereira RO, McCrory MA, Nye BG, Benavides GA, Darley-Usmar VM, Shioi T, Weimer BC, Abel ED. Enhanced cardiac Akt/protein kinase B signaling contributes to pathological cardiac hypertrophy in part by impairing mitochondrial function via transcriptional repression of mitochondrion-targeted nuclear genes. *Mol Cell Biol*. 2015;35:831-846. doi:10.1128/MCB.01109-14.
37. McMullen JR, Sherwood MC, Tarnavski O, Zhang L, Dorfman AL, Shioi T, Izumo S. Inhibition of mTOR signaling with rapamycin regresses established cardiac hypertrophy induced by pressure overload. *Circulation*. 2004;109:3050-3055. doi:10.1161/01.CIR.0000130641.08705.45.
38. Shioi T, McMullen JR, Tarnavski O, Converso K, Sherwood MC, Manning WJ, Izumo S. Rapamycin attenuates load-induced cardiac hypertrophy in mice. *Circulation*. 2003;107:1664-1670. doi:10.1161/01.CIR.0000057979.36322.88.
39. Song NJ, Yun UJ, Yang S, Wu C, Seo CR, Gwon AR, Baik SH, Choi Y, Choi BY, Bahn G, Kim S, Kwon SM, Park JS, Baek SH, Park TJ, Yoon K, Kim BJ, Mattson MP, Lee SJ, Jo

- DG, Park KW. Notch1 deficiency decreases hepatic lipid accumulation by induction of fatty acid oxidation. *Sci Rep*. 2016;6:19377. doi:10.1038/srep19377.
40. Liu Z, Turkoz A, Jackson EN, Corbo JC, Engelbach JA, Garbow JR, Piwnica-Worms DR, Kopan R. Notch1 loss of heterozygosity causes vascular tumors and lethal hemorrhage in mice. *J Clin Invest*. 2011;121:800-808. doi:10.1172/JCI43114.
  41. Nielsen CM, Cuervo H, Ding VW, Kong Y, Huang EJ, Wang RA. Deletion of Rbpj from postnatal endothelium leads to abnormal arteriovenous shunting in mice. *Development*. 2014;141:3782-3792. doi:10.1242/dev.108951.
  42. Yan M, Callahan CA, Beyer JC, Allamneni KP, Zhang G, Ridgway JB, Niessen K, Plowman GD. Chronic DLL4 blockade induces vascular neoplasms. *Nature*. 2010;463:E6-7. doi:10.1038/nature08751.
  43. Chi X, Shetty SK, Shows HW, Hjelmaas AJ, Malcolm EK, Davies BS. Angiopoietin-like 4 Modifies the Interactions between Lipoprotein Lipase and Its Endothelial Cell Transporter GPIHBP1. *J Biol Chem*. 2015;290:11865-11877. doi:10.1074/jbc.M114.623769.
  44. Yu X, Burgess SC, Ge H, Wong KK, Nasseem RH, Garry DJ, Sherry AD, Malloy CR, Berger JP, Li C. Inhibition of cardiac lipoprotein utilization by transgenic overexpression of Angptl4 in the heart. *Proc Natl Acad Sci U S A*. 2005;102:1767-1772. doi:10.1073/pnas.0409564102.
  45. Nakajima H, Ishida T, Satomi-Kobayashi S, Mori K, Hara T, Sasaki N, Yasuda T, Toh R, Tanaka H, Kawai H, Hirata K. Endothelial lipase modulates pressure overload-induced heart failure through alternative pathway for fatty acid uptake. *Hypertension*. 2013;61:1002-1007. doi:10.1161/HYPERTENSIONAHA.111.201608.
  46. Iso T, Maeda K, Hanaoka H, Suga T, Goto K, Syamsunarno MR, Hishiki T, Nagahata Y, Matsui H, Arai M, Yamaguchi A, Abumrad NA, Sano M, Suematsu M, Endo K, Hotamisligil GS, Kurabayashi M. Capillary endothelial fatty acid binding proteins 4 and 5 play a critical role in fatty acid uptake in heart and skeletal muscle. *Arterioscler Thromb Vasc Biol*. 2013;33:2549-2557. doi:10.1161/ATVBAHA.113.301588.

## Figure Legends

### Figure 1. Notch1 expression in the vasculature and cardiac effects of Dll4 blocking antibodies.

(A) Sections of gastrocnemius muscle, heart, liver and peri-gonadal white adipose tissue (WAT), from adult C57BL/6 mice stained against Notch1 (green). Endothelial cells were stained with TRITC-IB<sub>4</sub>-lectin (*Griffonia simplicifolia*) (red) and nuclei were stained with DAPI (blue). Scale bar, 100  $\mu$ m.

(B) Antibody staining against activated Notch1 (Notch1-ICD; brown) in left ventricular wall of adult C57BL/6 mice counterstained with Hematoxylin. Representative images shown; scale bar, 100  $\mu$ m.

(C-I) Adult C57BL/6 mice were treated with Dll4 neutralizing antibodies and control antibodies for eight weeks. (C) mRNA expression levels of the Notch target genes *Hey1* and *Hey2* in freshly isolated lung endothelial cells. (D) Heart weight in relation to body mass. (E-I) Transthoracic echocardiography of five control treated mice and five mice (labeled 1-5) treated with Dll4 antibodies. LVID, left ventricle inner diameter during systole and diastole. Mean and SEM shown; \* $p < 0.05$ ; n.s., not significant.

### Figure 2. Endothelial-specific *Rbpj* inactivation causes cardiac hypertrophy and heart failure.

(A, B) H&E staining of hearts shows cardiac hypertrophy 7 weeks after *Rbpj* gene recombination. Scale bar 25  $\mu$ m (A), 1 mm (B).

(C) Electron micrographs of hearts 8 weeks after gene recombination (L, lipid droplet; C, cardiac muscle; M, mitochondrion). Scale bar 500 nm.

(D) ATP in heart lysates 8 weeks after gene inactivation (n=10 control and 11 *Rbpj*<sup>iΔEC</sup> mice).

(E) Relative organ mass 8 weeks after *Rbpj* recombination (n=4 control and n=5 *Rbpj*<sup>iΔEC</sup> mice).

(F – I) Eight weeks after gene recombination, transthoracic echocardiography shows impaired heart function in *Rbpj*<sup>iΔEC</sup> mice (LVIDs left ventricle inner diameter during systole, n=5 mice).

(J) Transcript levels of the cardiac hypertrophy and heart failure marker *Bnp* (natriuretic peptide type B) and markers of the fetal cardiac gene expression program in heart lysates (*Col3a1*, type III collagen; *Myh6*, alpha myosin heavy chain; *Glut4*, glucose transporter-4; *Pdk2*, pyruvate dehydrogenase kinase isozyme-2; *Acadl*, acyl-Coenzyme-A dehydrogenase long-chain; *Acadm*, acyl-Coenzyme A dehydrogenase medium chain; *Cs*, citrate synthase; *Cpt1b*, carnitine palmitoyltransferase-1b muscle; n=4).

Mean and SEM or representative pictures shown, box plot depicts median and percentiles (10th, 25th, 75th, 90th); \*p<0.05, \*\*\*p<0.001.

**Figure 3. Endothelial-specific *Rbpj* inactivation increases cardiac vessel density.**

(A) Staining sections of heart (left ventricular wall), gastrocnemius muscle and brain against the endothelial marker CD31 at 4 and 8 weeks after gene recombination. 4 weeks after endothelial *Rbpj* gene recombination there were areas of normal vascular morphology and such with increased vessel size and vessel density (representative pictures shown).

(B-D) Quantification of the CD31-positive to total area in heart, muscle and brain 4 (n=3 mice) and 7 weeks after gene recombination (n=5 mice).

(E) mRNA expression of *CD31*, *Vegfr2* and *Vegf-a* in heart lysates of *Rbpj*<sup>iΔEC</sup> and control mice 7 weeks after gene recombination (n=4 mice).

(F) Blood perfusion in the ear skin determined by laser-doppler analysis 7 weeks after gene recombination (n=6 control and 7 *Rbpj*<sup>iΔEC</sup> mice).

(G) Hoechst dye 33342 (blue) was injected into a tail vein 7 weeks after gene recombination (n=5 mice) and mice sacrificed 60 seconds later. Fixed heart sections were counterstained with nuclear red to identify cell nuclei to which the dye was transported (representative images).

Scale bars 50 μm. Mean and SEM shown. \*p<0.05, \*\*\*p<0.001.

**Figure 4. Endothelial Notch signaling regulates systemic lipid clearance.**



(A) H&E staining of pancreatic islets and liver.

(B, C) Non-esterified fatty acids (NEFA) and plasma triacylglyceride (TAG) concentration 6 weeks after endothelial *Rbpj* gene inactivation (n=5 mice).

(D) Liver lipid content quantified by determination of Oil Red O stained droplets (n=3 mice).

(E – F) Hepatic expression of key genes involved in lipogenesis and lipolysis (n≥3 mice).

(G) Hepatic TAG secretion of *Rbpj*<sup>iΔEC</sup> mice and controls (n=6 mice).

(H-K) At 4-5 weeks after gene recombination, fat clearance test with oral gavage of olive oil (n=6 control and 7 *Rbpj*<sup>iΔEC</sup> mice) shows impaired TAG clearance in *Rbpj*<sup>iΔEC</sup> mice after serum TAG levels reached their highest level. Clearance rate was calculated as slope from maximum to end. Defecation and TAG content of feces (n=4). Mean and SEM or representative pictures shown, Scale bar 100 μm, \*p<0.05, \*\*p<0.01, \*\*\*p<0.001.

**Figure 5. EC-specific *Rbpj* ablation disturbs fatty acid transport.**

- (A) Plasma lipase activity after heparin injection was diminished in *Rbpj*<sup>iΔEC</sup> mice (n=3).
- (B,C) Uptake of the long-chain fatty acid (FA) analogue <sup>3</sup>H-R-bromopalmitate into muscle tissue but not liver and white adipose tissue (WAT) was impaired in *Rbpj*<sup>iΔEC</sup> mice 5 weeks after gene recombination. Weighted averaged activity of the <sup>3</sup>H-R-bromopalmitate tracer during the uptake experiment (n=6 mice).
- (D, E) Concentration of acyl-CoA in several tissues (n=10 control and 7 *Rbpj*<sup>iΔEC</sup> mice) and of acyl-carnitines with different chain length in heart (n=5 control and 4 *Rbpj*<sup>iΔEC</sup> mice).
- (F) Uptake of fluorescently labeled palmitic acid (FA-BODIPY) into primary human venous EC (HUVEC) upon Notch signaling inhibition (DAPT) or activation (Dll4 coating). n=3. Mean and SEM shown, \*p<0.05, \*\*p<0.01, \*\*\*p<0.001.

**Figure 6. Notch signaling controls transcription of genes involved in endothelial TAG hydrolysis and transport of fatty acids.**

- (A) Expression of genes involved in uptake and transendothelial shuttling of fatty acids in HUVEC upon genetic Notch manipulation (*LIPG*, *lipase G, endothelial type*; *ANGPTL4*, *angiopoietin like 4*; *solute carrier family 27 member 4* and *acyl-CoA synthetase long-chain family member 1, 3, 5* (*FATP4*, *ACSL1*, 3, 5; *FABP*, *fatty acid binding protein*) (n=3).
- (B) Expression of *Gpihbp1* (*glycosylphosphatidylinositol anchored high density lipoprotein binding protein-1*) in primary heart ECs isolated from controls and *Rbpj*<sup>iΔEC</sup> mice (n=4).
- (C) Expression of *Angptl4* and *CD36* mRNA in freshly isolated lung and heart ECs (n=3 control and 4 *Rbpj*<sup>iΔEC</sup> mice).

**(D, E)** Western blotting to determine expression of Angptl4 and CD36 protein in primary murine heart endothelial cells overexpressing GFP, dnMAML to block Notch activity or Notch1-ICD.

**(F)** Uptake of fluorescently labeled palmitic acid (FA-BODIPY) into HUVEC upon forced CD36 expression (n=4).

**(G)** Expression of FABP4 protein in primary murine heart endothelial cells overexpressing GFP, Notch1-ICD or dnMAML.

**(H)** Expression of *FABP4*, *ANGPTL4* and *CD36* mRNA upon Notch manipulation in the presence of 1 $\mu$ M T0070907 (PPAR $\gamma$  inhibitor) in HUVEC (n=3).

**(I)** Enrichment of DNA from a putative Rbpj-binding motif in the CD36 promoter of HUVEC after precipitation with an antibody recognizing Rbpj (representative experiment).

Results are shown as mean and SEM or representative pictures, \*p<0.05, \*\*p<0.01, \*\*\*p<0.001.

**Figure 7. Elevated glucose uptake and metabolism in *Rbpj* <sup>$\Delta$ EC</sup> hearts.**

**(A, B)** Uptake of <sup>18</sup>F-fluoro-2-deoxy-D-glucose into hearts (SUV, standardized uptake value, n=10 mice).

**(C)** Glucose-6-phosphate (G-6-P) in heart, gastrocnemius muscle, liver and peri-gonadal white adipose tissue (WAT) of control and *Rbpj* <sup>$\Delta$ EC</sup> mice (n=7).

**(D – F)** Concentration of several carbohydrates and pyruvate in hearts (n=5) or plasma (n=7 control and 3 *Rbpj* <sup>$\Delta$ EC</sup> mice).

Mean and SEM, box plot depicts median and percentiles (10th, 25th, 75th, 90th), \*p<0.05, \*\*p<0.01.

**Figure 8. Reducing glucose metabolism by ketogenic diet prevents failure of *Rbpj*<sup>iΔEC</sup> hearts.**

**(A)** Phosphorylation of several kinases from the insulin, AMPK (AMP-activated protein kinase) and mTOR (mechanistic target of rapamycin) pathways in hearts of *Rbpj*<sup>iΔEC</sup> mice (PRAS40, proline-rich AKT1 substrate 1; S6K, ribosomal protein S6 kinase beta-1; S6, ribosomal protein S6; ERK, mitogen-activated protein kinase; AKT, protein kinase B; BAD, bcl2-associated agonist of cell death; antibody array, n=4 hearts).

**(B)** From 8 to 11 weeks after gene recombination, *Rbpj*<sup>iΔEC</sup> and control mice were either treated with rapamycin and control diet, vehicle and ketogenic diet, or vehicle and control diet. Mice receiving ketogenic diet were additionally pretreated with high fat diet for 2 weeks (n=4 control and 5 *Rbpj*<sup>iΔEC</sup> mice).

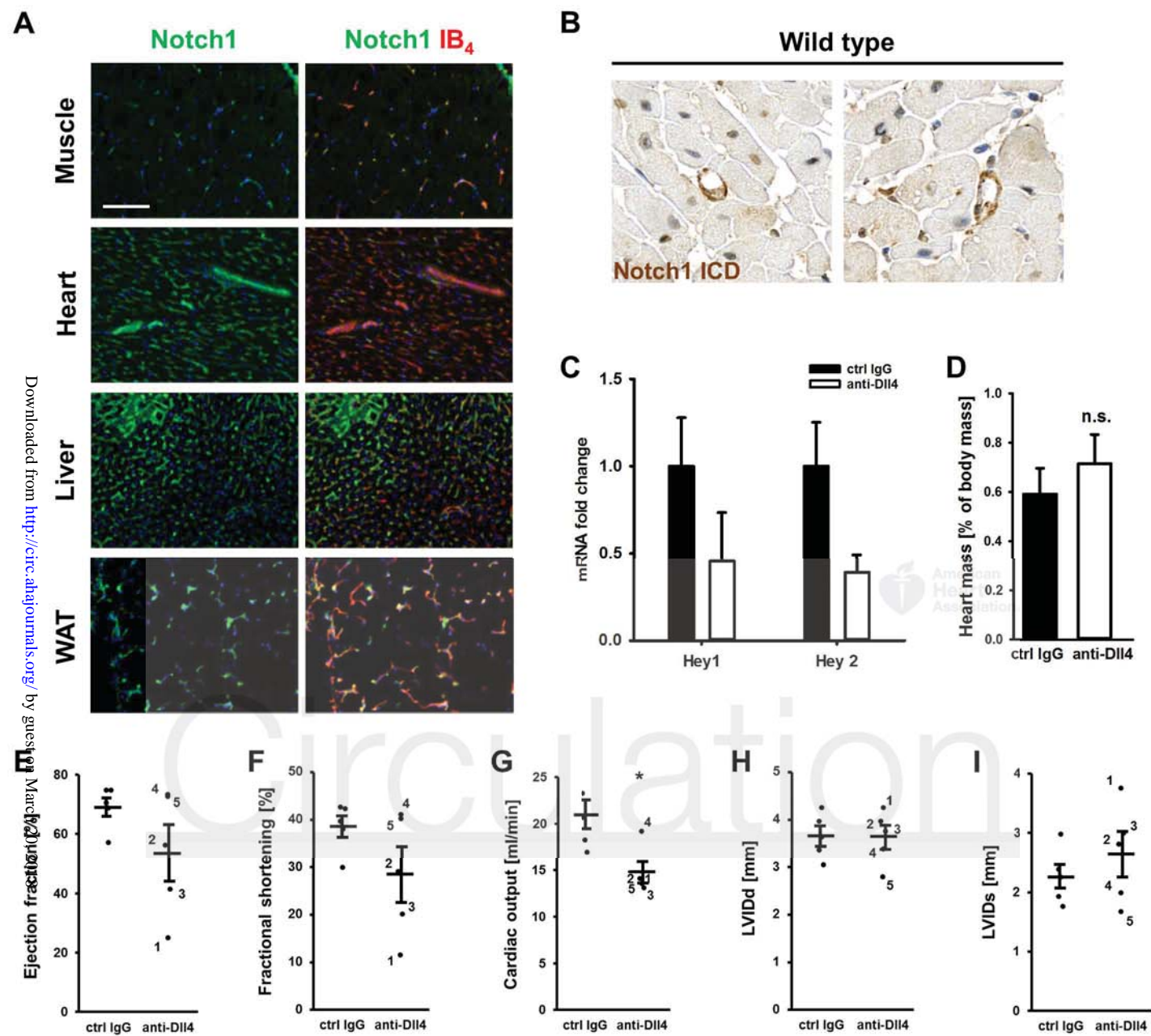
**(C)** Heart-to-body weight ratio.

**(D – G)** *Rbpj*<sup>iΔEC</sup> and control mice were fed with ketogenic and control diet starting with gene recombination (n≥4 mice).

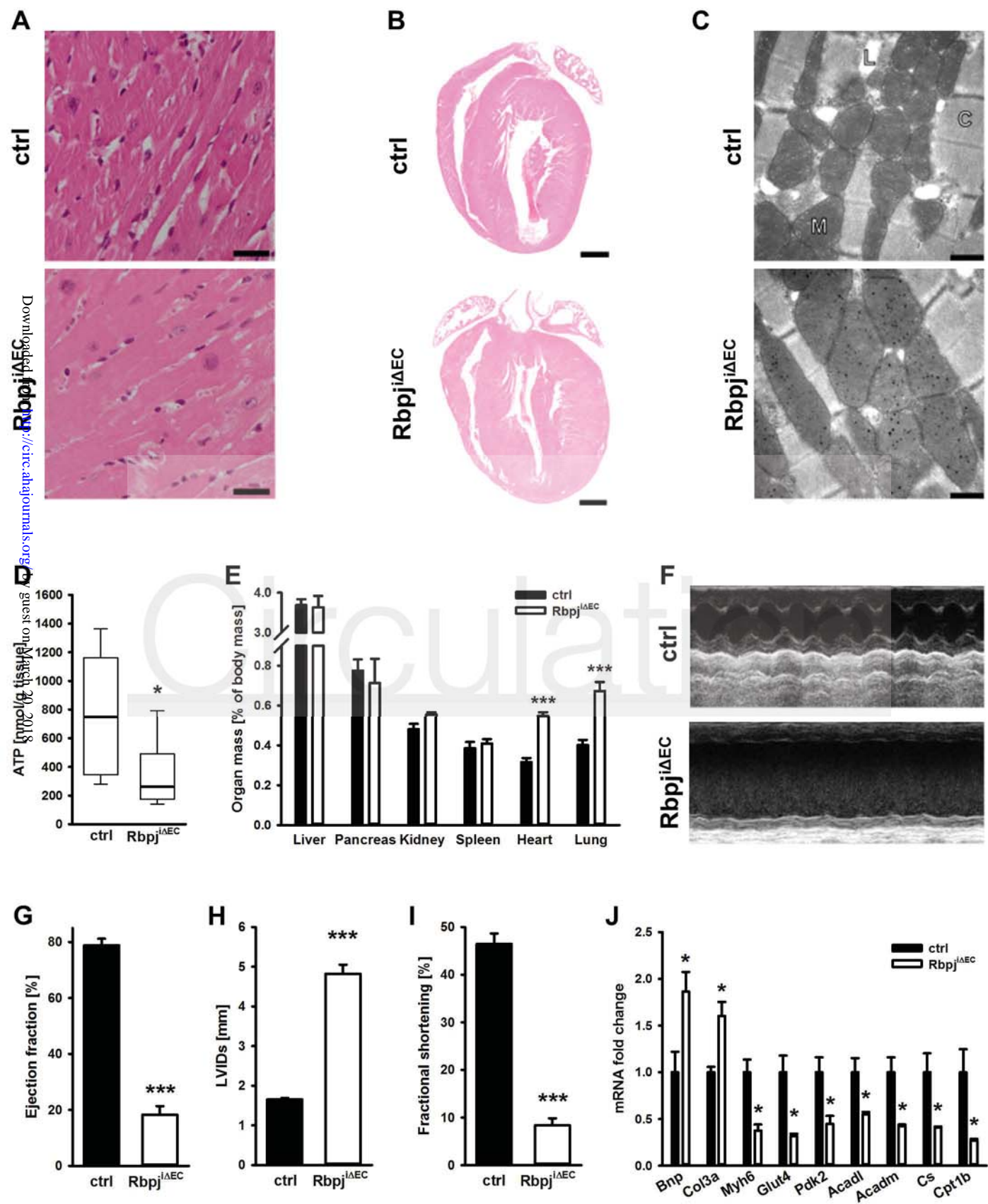
**(E-G)** Transthoracic echocardiography (n≥4 mice; LVIDs left ventricle inner diameter during systole).

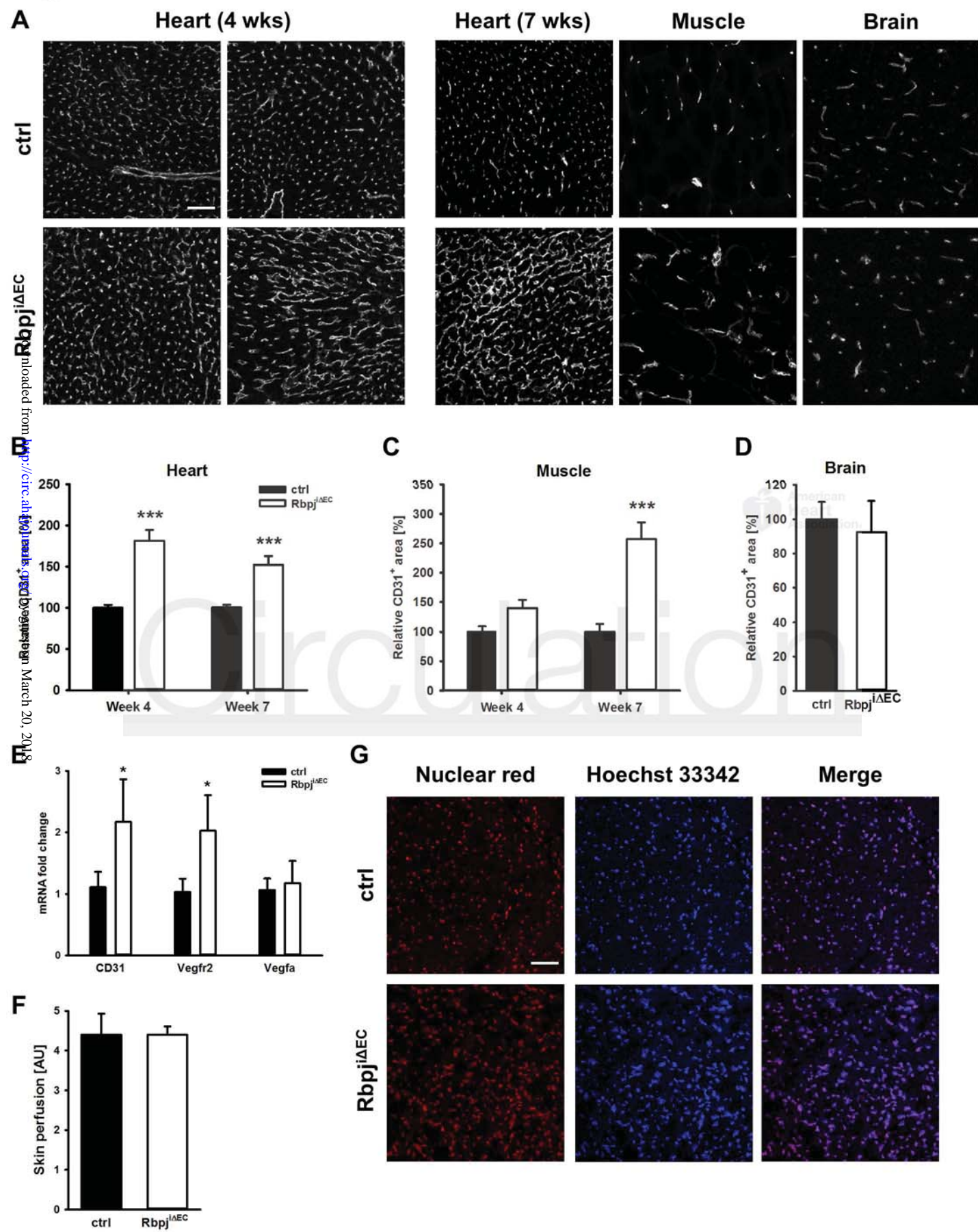
**(H)** Glucose-6-phosphate (G-6-p) levels in hearts from mice kept on control or ketogenic diet (n=4).

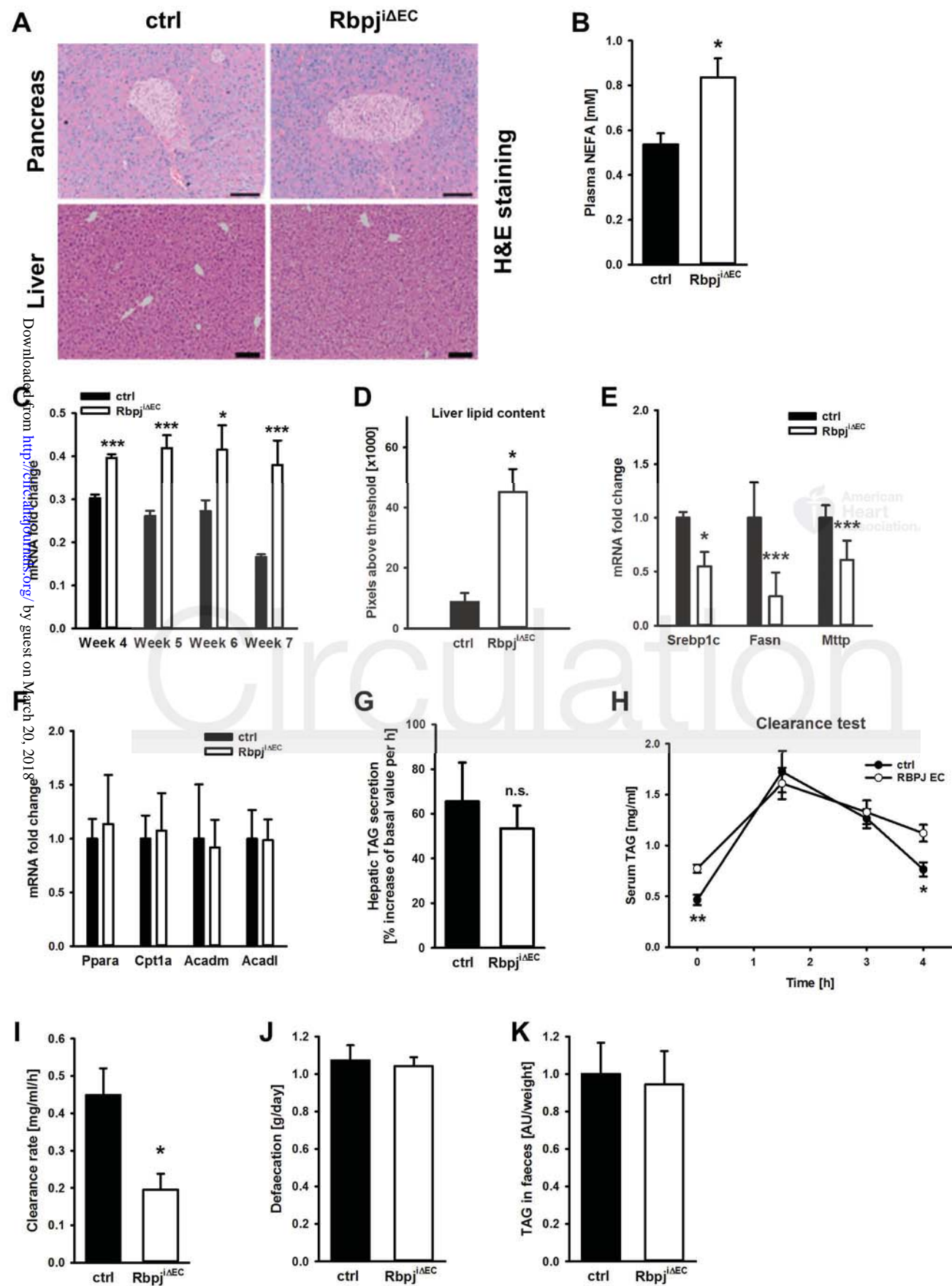
Mean and SEM or representative pictures shown, \*p<0.05, \*\*p<0.01, \*\*\*p<0.001.

**Fig. 1**

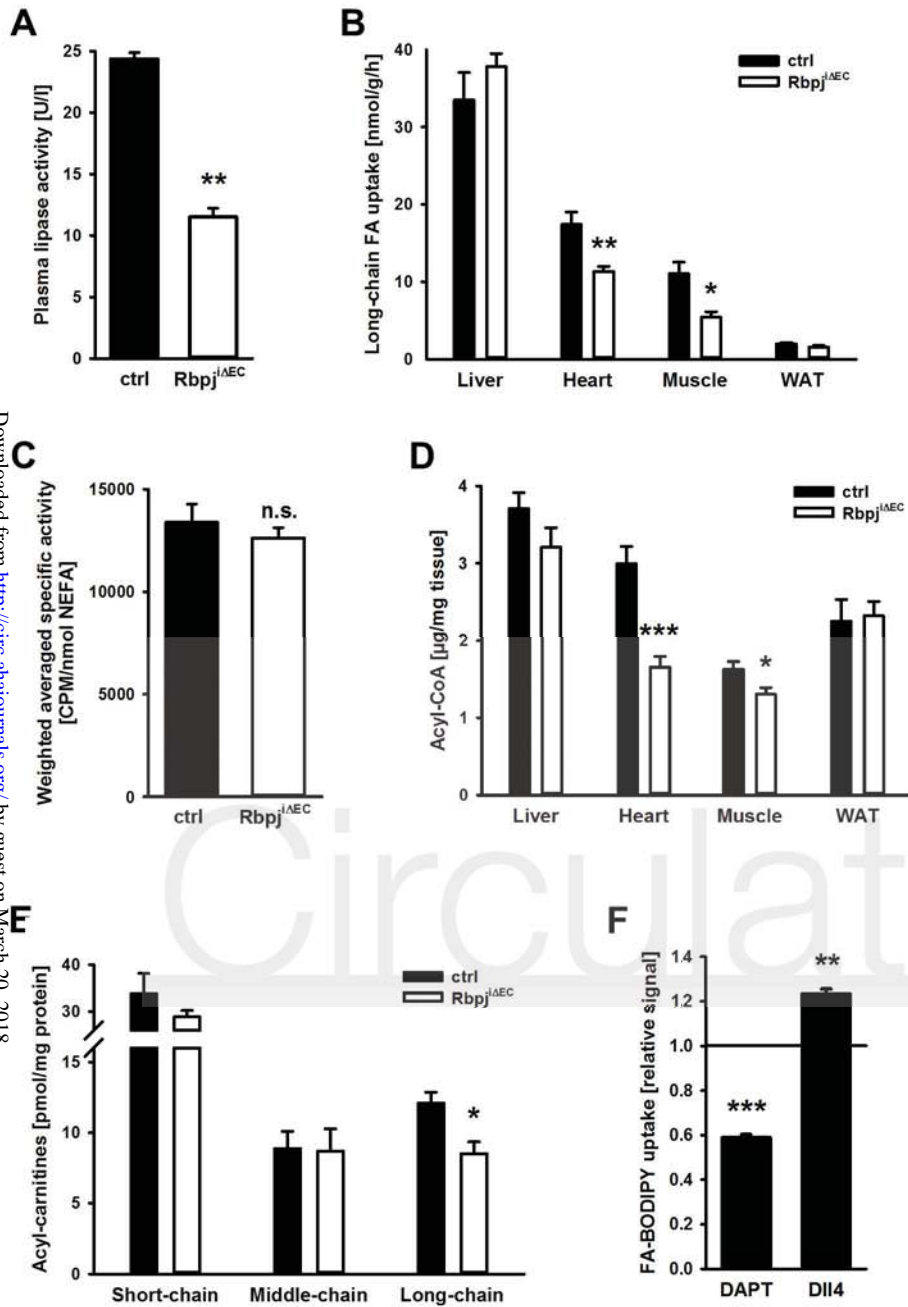
**Fig. 2**



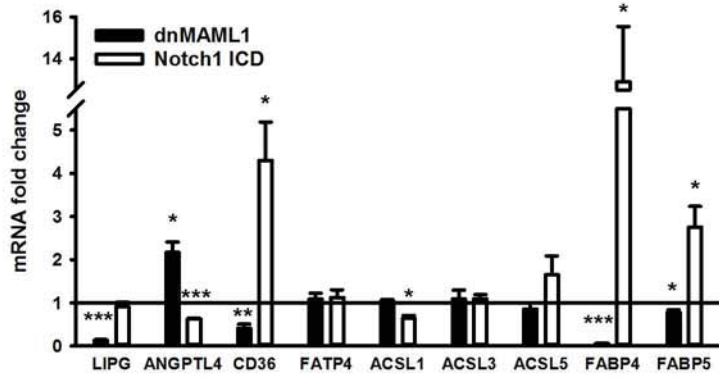
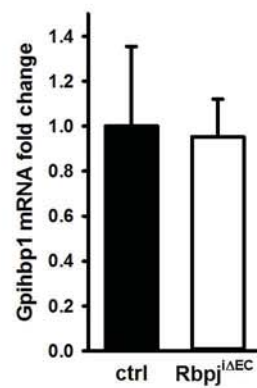
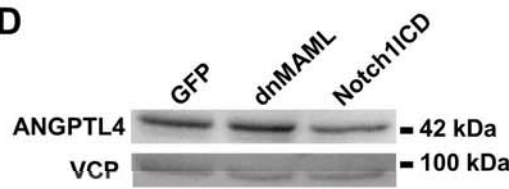
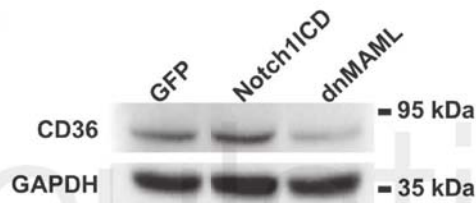
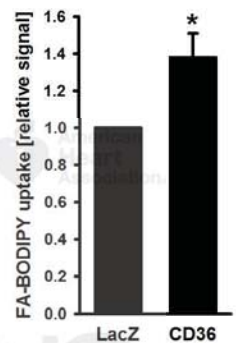
**Fig. 3**

**Fig. 4**

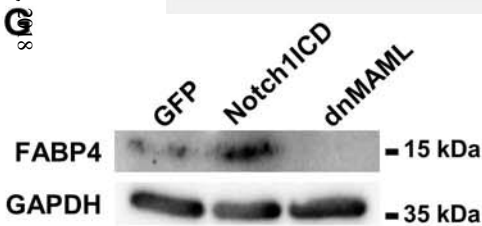
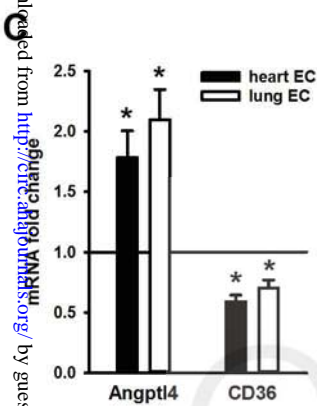
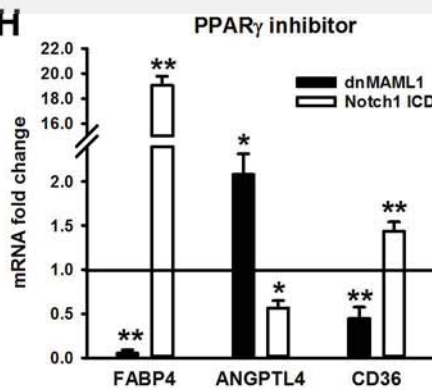
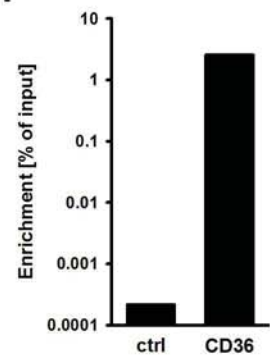
# Fig. 5



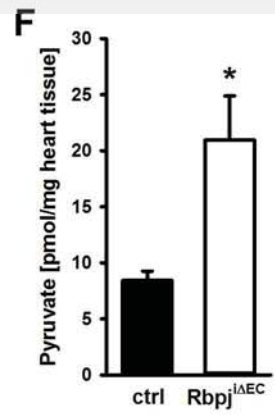
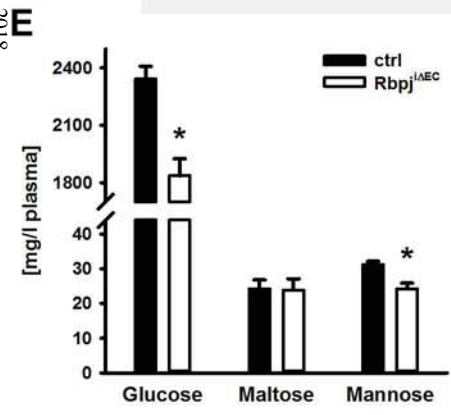
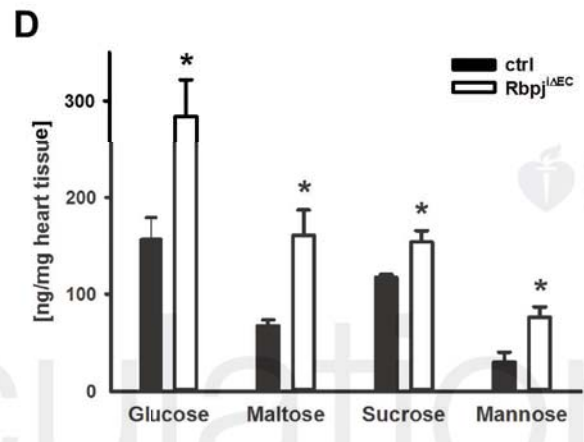
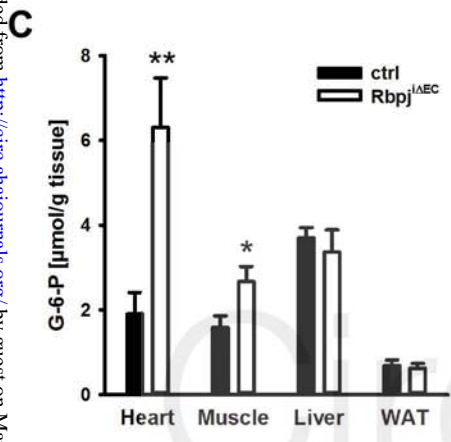
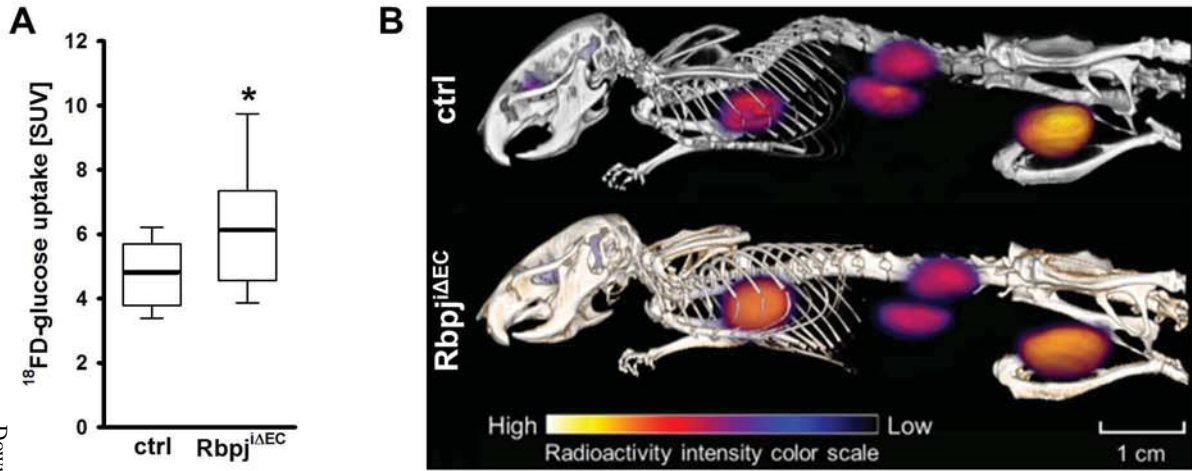
Circulation

**Fig. 6****A****B****D****E****F**

Downloaded from <http://circ.ahajournals.org/> by guest on March 20, 2018

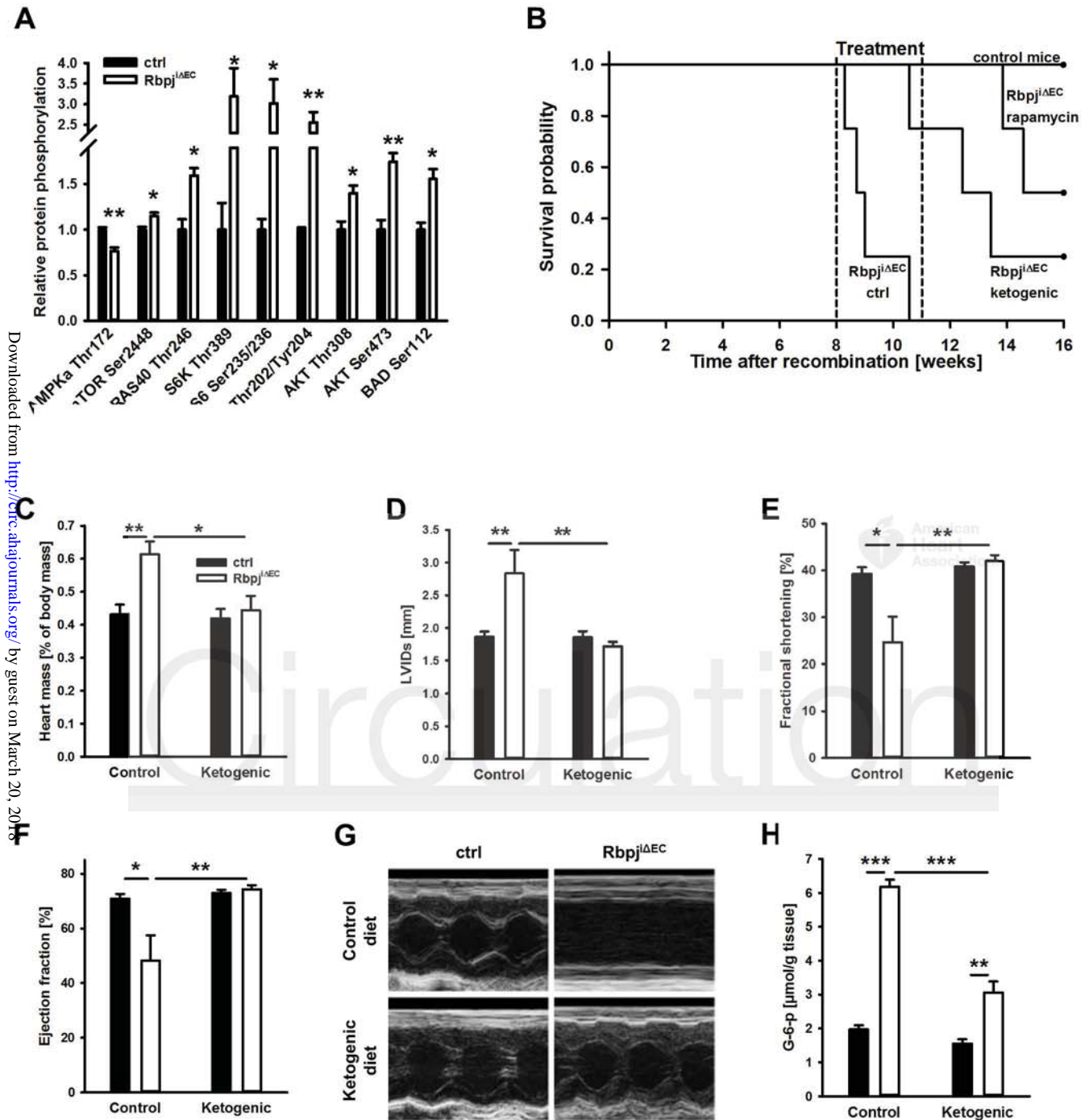
**H****I**

# Fig. 7



Downloaded from <http://circ.ahajournals.org/> by guest on March 20, 2018



**Fig. 8**

## **Inhibition of Endothelial Notch Signaling Impairs Fatty Acid Transport and Leads to Metabolic and Vascular Remodeling of the Adult Heart**

Markus Jabs, Adam J. Rose, Lorenz H. Lehmann, Jacqueline Taylor, Iris Moll, Tjeerd P. Sijmonsma, Stefanie E. Herberich, Sven W. Sauer, Gernot Poschet, Giuseppina Federico, Carolin Mogler, Eva-Maria Weis, Hellmut G. Augustin, Minhong Yan, Norbert Gretz, Roland M. Schmid, Ralf H. Adams, Hermann-Joseph Gröne, Rüdiger Hell, Jürgen G. Okun, Johannes Backs, Peter P. Nawroth, Stephan Herzig and Andreas Fischer

*Circulation*. published online January 20, 2018;

*Circulation* is published by the American Heart Association, 7272 Greenville Avenue, Dallas, TX 75231

Copyright © 2018 American Heart Association, Inc. All rights reserved.

Print ISSN: 0009-7322. Online ISSN: 1524-4539

The online version of this article, along with updated information and services, is located on the World Wide Web at:

<http://circ.ahajournals.org/content/early/2018/01/17/CIRCULATIONAHA.117.029733>

Data Supplement (unedited) at:

<http://circ.ahajournals.org/content/suppl/2018/01/17/CIRCULATIONAHA.117.029733.DC1>

**Permissions:** Requests for permissions to reproduce figures, tables, or portions of articles originally published in *Circulation* can be obtained via RightsLink, a service of the Copyright Clearance Center, not the Editorial Office. Once the online version of the published article for which permission is being requested is located, click Request Permissions in the middle column of the Web page under Services. Further information about this process is available in the [Permissions and Rights Question and Answer](#) document.

**Reprints:** Information about reprints can be found online at:  
<http://www.lww.com/reprints>

**Subscriptions:** Information about subscribing to *Circulation* is online at:  
<http://circ.ahajournals.org/subscriptions/>

# SUPPLEMENTAL MATERIAL

**Jabs et al., Inhibition of endothelial Notch signaling impairs fatty acid transport and leads to metabolic and vascular remodeling of the adult heart**

**Corresponding author:**

Andreas Fischer, MD

German Cancer Research Center

Vascular Signaling and Cancer (A270)

Im Neuenheimer Feld 280

69210 Heidelberg, Germany

FAX: +49 6221 42 4159

Phone: +49 6221 42 4150

Email: [a.fischer@dkfz.de](mailto:a.fischer@dkfz.de)

**Contents:**

Supplemental Methods

Supplementary Figures 1 – 5

Supplementary References

Supplementary Movie legend

## Supplementary Methods

### Experimental animals

Rbpj<sup>iΔEC</sup> mice (Cdh5-CreERT2,Rbpj<sup>lox/lox</sup>) were obtained by crossing Cdh5-CreERT2 mice with Rbpj<sup>lox/lox</sup> mice.<sup>1</sup> Rbpj<sup>iΔEC</sup> mice and controls were injected 1.5 mg tamoxifen i.p. for 5 consecutive days. Gene recombination was induced at an age of 6 to 10 weeks. Animals were group housed under specific-pathogen-free condition. Littermates were randomly assigned to experimental groups. All animal experiments were performed according to the guidelines of the local institution and the local government (Regierungspräsidium Karlsruhe).

### Cell culture

Neonatal rat cardiomyocytes were isolated and cultured as described previously.<sup>2</sup> HUVEC were grown and maintained until passage 5 in Endopan-3 Growth Medium containing 3% FCS and supplements (Pan-Biotech). For isolation of lung microvascular EC, lungs were minced and digested with 0.5 mg/ml collagenase for 2 hours. Larger tissue remnants were filtered out and the cell suspension was incubated for 1 hour with beads coupled to CD31 antibodies (Pharmingen). Microvascular ECs were isolated from hearts by mincing the ventricles and digesting them for 1 hour with 2 mg/ml collagenase and 2.4 mg/ml dispase II. Larger tissue remnants were filtered out and the cell suspension was incubated for 1h with beads coupled to CD31-antibodies (Pharmingen). After four times washing, the cells were separated from the beads with trypsin, spun down and snap-frozen in liquid nitrogen for RNA analysis or were cultured for viral transduction. Primary brain ECs were isolated as described previously.<sup>3</sup> All cells were isolated from individuals of both sexes and were cultivated at 37 °C and 5% carbon dioxide.

### Viral transduction

HUVEC were transduced with adenoviral vectors at a MOI of 50. The vectors encoding dominant-negative MAML1, Notch1 intracellular domain, and GFP were described earlier.<sup>4, 5</sup>

### qPCR analysis

RNA was isolated using the innuPREP RNA Mini kit (Analytik Jena). cDNA was synthesized with the High-Capacity cDNA Reverse Transcription Kit (Applied Biosystems). The cDNA was applied to qPCR using the POWER SYBR Green Master Mix (Applied Biosystems). Gene expression was assessed by  $2^{-\Delta\Delta ct}$ -method and normalized with the genes RPS29, HPRT1 (human) and RPL32, LMNA (mouse).

### Western blotting and antibody array

For protein analysis, cells were lysed in RIPA buffer containing a proteinase and phosphatase inhibitor (both from Roche), 1 mM DTT and 2 mM  $\text{Na}_3\text{VO}_4$ . Proteins were electrophoresed on SDS gels and were transferred to nitrocellulose membranes, which were then blocked in 5% skim milk or BSA in TBS containing 0.05% Tween-20. The membranes were incubated with primary antibodies overnight, washed and incubated for 1 hour with peroxidase-conjugated secondary antibody (Dako) at room temperature. Images were acquired with a ChemiDoc imaging system and quantified with Image Lab software (both Bio-Rad). The following primary antibodies were used: RBPJ, FABP4, ANGPTL4, p-S6, p-S6K (from Cell Signaling), VCP, GAPDH, CD36 (from Abcam).

The antibody array was purchased from Cell Signaling (PathScan Intracellular Signaling Array Kit, chemiluminescent readout). Tissues were snap frozen, weighted and equal amounts homogenized in the supplied lysis buffer. The lysates were diluted to equal protein concentration and a Coomassie gel was run as control. Then the array was performed according to the manufacturer's instructions.

### Fatty acid-BODIPY uptake

Uptake of fluorescently labeled fatty acids was essentially carried out as described (Hagberg et al., 2010). Basal medium supplemented with 1% fatty acid-free BSA was used during the experiments. HUVEC were seeded either directly in a 24-well plate and were incubated overnight with 25  $\mu\text{M}$  DAPT (N-[(3,5-difluorophenyl)acetyl]-L-alanyl-2-phenyl]glycine-1,1-dimethylethylester; Calbiochem) or DMSO, or they were seeded on plates coated with IgG or human DLL4 24 h before the experiment was carried out. For the coating recombinant human DLL4 protein (2.5  $\mu\text{g}$ ; R&D) or 2.5  $\mu\text{g}$  IgG as control (Rockland) were diluted in 1 mL 0.1%

gelatin in phosphate buffered saline. 24 well dishes were coated with 200  $\mu$ l of this mixture for 12 h at 4°C. The coated wells were washed with PBS before seeding the cells. The day after seeding, the cells were washed with PBS containing 1% fatty acid-free BSA. Then, they were incubated for 3 minutes with PBS / fatty acid-free BSA containing 20  $\mu$ M 4,4-Difluoro-5,7-Dimethyl-4-Bora-3a,4a-Diaza-s-Indacene-3-Hexadecanoic Acid (BODIPY-C16, Life Technologies) at 37 °C. Then the cells were washed twice with PBS and fixed 10 minutes with 4% PFA. The fixed cells were covered with PBS and were immediately imaged with a wide field fluorescence microscope using a 5X objective. At least 30 images were taken from different positions of each well. The signal intensity was quantified with ImageJ.

### Chromatin IP

HUVEC were grown on 15 cm culture plates until 90% confluency and fixed with 1% formaldehyde. Cells were then lysed in RIPA buffer and sonicated for 10 cycles (30 s ON, 30 s OFF) using a Bioruptor Pico (Diagenode), which yielded DNA fragments of 200-1000 bp. Chromatin samples were incubated with antibodies directed against RBPJ (Cell Signaling) at 4 °C overnight and immunoprecipitated chromatin fragments were purified using Protein-G magnetic beads. Crosslinks were reversed at 65 °C overnight. After DNA purification (HP PCR Product Purification Kit, Roche), qPCR was performed with the primer sets TCTGAACCCTTTCGTTGGTAAT, TCCCTTAAATAACTGCGACCTT (bind approximately 1.3 kb upstream of the transcript variant NM\_000072) and GAAGTGGTGCTTCCAGGTCA, GGTGATTTTGAAGCAGGCGG (bind within intron 3 of transcript NM\_000072, which is assumed to not have regulatory functions). Enrichment was calculated by the percent input method. The antibody was tested for specificity by western blot and the beads alone did not enrich DNA.

### Histology

Glycogen was visualized on paraffin-embedded sections by Periodic Acid Schiff staining. The sections were deparaffinized and rehydrated. Then the slides were incubated in 0.5% periodic acid for 5 minutes, rinsed with water and incubated with Schiff's reagent (Carl Roth) for 15 minutes. Subsequently the slides were rinsed with tap water for 10 minutes, stained with hemalum and rinsed again for 5 minutes. For HE staining, sections were deparaffinized and

rehydrated, then stained for 2 minutes in hematoxylin, incubated in tap water for 10 minutes, stained for 30 seconds with eosin and were washed in tap water again.

For electron microscopy, hearts were fixed in Karnovsky's solution, followed by postfixation in 2% osmium tetroxide, and were then embedded in Araldite (Polysciences). Ultrathin sections have been cut 60 to 70 nm with a Leica Ultracut UCT (Leica Microsystems), were counterstained with uranyl acetate and lead citrate, and were analyzed with an EM900 (Zeiss).

Blood vessels were stained with TRITC-lectin on cryosections. PFA-fixed sections were blocked with 10% goat serum for 1 h and incubated with TRITC-lectin 1:100 in PBlec (PBS pH 6.8, 0.1 mM CaCl<sub>2</sub>, 0.1 mM MgCl<sub>2</sub>, 0.1 mM MnCl<sub>2</sub>, 1% Triton X-100). After washing three times with PBlec, the sections were stained with DAPI in PBS, washed twice with PBS and were mounted. Notch1 was stained with a polyclonal antibody (R&D Systems) on paraffin embedded sections. After rehydrating the sections, they were blocked with 5% BSA in TBS-T and were incubated with the 1st antibody (1:30 in blocking solution overnight). Then the sections were washed TBS-T and incubated for 2 h with TRITC-lectin and 2<sup>nd</sup> antibody coupled to a fluorophore (1:100 and 1:200 in PBlec respectively). Staining with antibodies detecting LYVE1, CD36, Notch1 ICD (Abcam) and Angptl4 (Life Technologies) was performed similarly but with additional heat-mediated antigen retrieval at pH 6.

### Metabolic tests

Mice were generally kept on chow diet. When indicated, mice were fed a ketogenic diet (0.2% carbohydrates, 67% fat, 18% proteins per weight, D12369Bi, Research Diets) or a control diet (67% carbohydrates, 4% fat, 19% proteins per weight, D12450Bi, Research Diets). TAG, total ketone bodies and NEFA were measured using kits from Sigma and Wako Diagnostics respectively. Glucose-6-phosphate was determined with a kit from Cayman Chemical Company. Acyl-CoAs were extracted from tissues (Golovko and Murphy, 2004) and detected (Barber and Lands, 1971). Acyl-carnitines were determined by homogenizing tissues in water and analyzing the lysate by electrospray ionization tandem mass spectrometer (Sauer et al., 2006). Lipase activity was determined with the fluorescence-based Lipase Activity Assay Kit (Cayman) in plasma drawn 5 minutes after injection of 50 U Na-heparin i.v. For the fat clearance test, mice were starved overnight. Blood was drawn before administration of 100 µl olive oil (Carl Roth) by oral gavage and at indicated time points. Long-chain FA uptake into organs was assessed as

described.<sup>6</sup> Mice were fasted for 20 hours before they received trace amounts of <sup>3</sup>H-R-bromopalmitate via tail vein. 2 and 15 minutes after injection, blood was collected to determine whether the ratio of radioactivity and NEFA concentration was similar in both experimental groups. 16 minutes after injection, tissues were harvested and radioactivity was determined in the lysates. Uptake of glucose to the heart was monitored by PET. After starvation for 4 hours, mice were anesthetized and received <sup>18</sup>F-fluoro-2-deoxy-D-glucose by tail vein injection (maximum dose 10 MBq). After ten minutes, the animals were measured in a multimodality PET/CT system (Inveon, Siemens) for ten minutes. For quantification the heart was gated as region that had an SUV higher than 60% of the local maximum SUV. To determine hepatic TAG secretion, mice were starved for 5 hours, before they were intravenously administered 500 mg/kg body weight Tyloxapol (Sigma). Blood was collected before injection and after 30, 60 and 90 minutes to determine TAG levels. Hepatic TAG secretion was calculated as increase of plasma TAG levels after 90 minutes relative to basal levels.

#### Quantification of metabolites by HPLC or GC

Aliquots (15-25 mg) of freshly ground murine tissue were used for absolute quantification of adenosine content. Adenosine compounds were extracted with 0.25 ml ice-cold 0.1 M HCl in an ultrasonic ice-bath for 10 min. The resulting homogenates were centrifuged for 10 min at 4°C and 16.400 g to remove cell debris. Adenosines were derivatized with chloroacetaldehyde as described in (Bürstenbinder et al., 2007) and separated by reversed phase chromatography on an Acquity BEH C18 column (150 mm x 2.1 mm, 1.7 µm, Waters) connected to an Acquity H-class UPLC system. Prior separation, the column was heated to 42°C and equilibrated with 5 column volumes of buffer A (5.7 mM TBAS, 30.5 mM KH<sub>2</sub>PO<sub>4</sub> pH 5.8) at a flow rate of 0.45 ml min<sup>-1</sup>. Separation of adenosine derivates was achieved by increasing the concentration of buffer B (2/3 acetonitrile in 1/3 buffer A) in buffer A as follows: 1 min 1% B, 1.6 min 2% B, 3 min 4.5% B, 3.7 min 11% B, 10min 50% B, and return to 1% B in 2 min. The separated derivates were detected by fluorescence (Acquity FLR detector, Waters, excitation: 280 nm, emission: 410 nm) and quantified using ultrapure standards (Sigma). Data acquisition and processing was performed with the Empower3 software suite (Waters).

Aliquots of freshly ground murine heart tissue were used for absolute quantification of  $\alpha$ -ketoacid and sugar content. For extraction of  $\alpha$ -ketoacids 300 µl 0.1M ice-cold HCl was used.

For derivatization of  $\alpha$ -ketoacids 150  $\mu$ l of the acidic extract was mixed with an equal volume of 25 mM o-phenyldiamine and incubated at 50°C for 30 minutes. The derivatized  $\alpha$ -ketoacids were separated using an Acquity HSS T3 column (100 mm x 2.1 mm, 1.7  $\mu$ m, Waters) connected to an Acquity H-class UPLC system. Prior separation, the column was heated to 40°C and equilibrated with solvent A (0.1% formic acid in 10% acetonitrile) at a flow rate of 0.55 ml/min. Separation of  $\alpha$ -ketoacid derivates was achieved by increasing the concentration of solvent B (acetonitrile) in solvent A as follows: 2 min 2% B, 5 min 18% B, 5.2 min 22% B, 9 min 40% B, 9.1min 80% B and hold for 2min, and return to 2% B in 2 min. The separated derivates were detected by fluorescence (Acquity FLR detector, Waters, excitation: 350 nm, emission: 410 nm) and quantified using ultrapure standards (Sigma). Data acquisition and processing was performed with the Empower3 software suite (Waters).

Sugars were extracted with 700  $\mu$ l ultra-pure water for 20 minutes at 95°C and were separated on a CarboPac PA1 column (ThermoScientific) connected to the ICS-5000 system and quantified by pulsed amperometric detection (HPAEC-PAD). Column temperature was kept constant at 25 °C and equilibrated with five column volumes of solvent A (ultra-pure water) at a flow rate of 1 ml/min. Baseline separation of carbohydrates was achieved by increasing the concentration of solvent B (300 mM NaOH) in solvent A as follows: From 0 to 25 min 7.4% B, followed by a gradient to 100% B within 12 min, hold for 8 min at 100% B, return to 7.4% B and equilibration of the column for 12 min. Data acquisition and quantification was performed with Chromeleon 7 (ThermoScientific).

### Echocardiography

Mice were not anesthetized during transthoracic echocardiography, which was performed essentially as described.<sup>2</sup>

### Perfusion and vascular permeability

Mice were anesthetized with ketamine / xylazine. 15 minutes after injection, the ears of the mice were shortly warmed with red light and the perfusion was measured by a laser Doppler system (Periflux 5000 with Integrating Probe 413, Perimed). The perfusion rate for each mouse was determined by taking the mean of six measurements.

To measure permeability in cell culture, HUVEC were seeded on cell culture inserts (pore size 0.4  $\mu\text{m}$ ), which had been coated with fibronectin. The next day, cells were transduced with adenoviral vectors. After 48 hours, the medium was changed and FITC-dextran was added to a concentration of 0.5 mg/ml to the upper compartment. An aliquot of medium was removed at the indicated time points and fluorescence was determined after dilution with PBS. For measurement of transendothelial electrical resistance (TER), HUVEC were cultured on fibronectin-coated transwell filters with 3  $\mu\text{m}$  pore size. TER and corresponding capacity (ccl) were measured every ten minutes with a CellZscope apparatus (nanoAnalytics, Münster, Germany).

To measure vascular permeability in the Miles Assay, 100  $\mu\text{l}$  Evans Blue (1% in saline) was injected into the tail vein. Then, the animals were anesthetized and PBS or histamine (100 ng) was injected intradermal. The animals were euthanized 20 minutes later and the skin surrounding the injection sites was removed, minced and incubated in 200  $\mu\text{l}$  formamide at 56°C for 48 hours. The absorbance of extracted Evans Blue was measured at 620 nm.

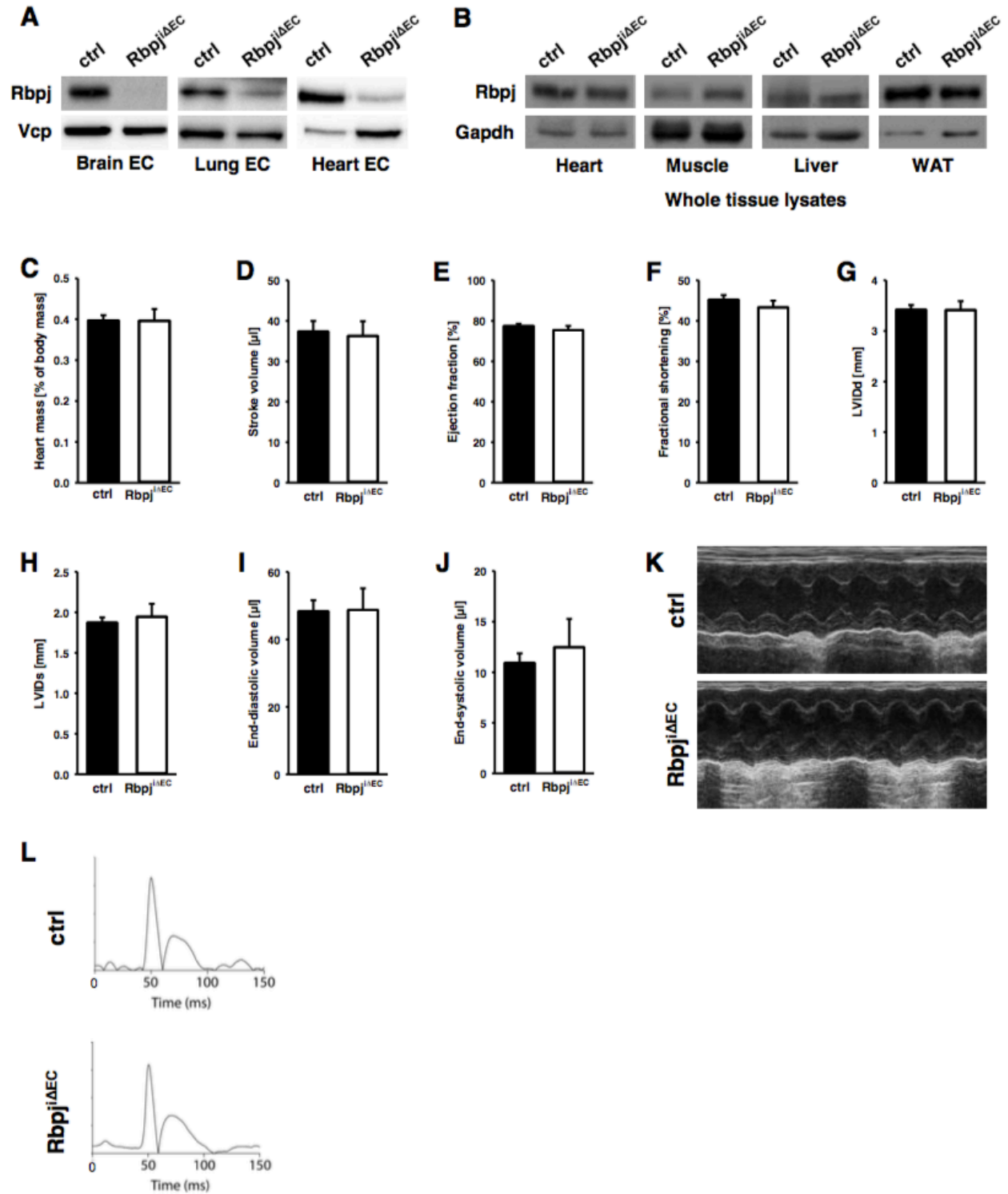
For the peritonitis assay, 100  $\mu\text{l}$  of 2 mg/ml FITC-dextran or TRITC-dextran (40 or 10 kDa respectively) were i.v. injected. 5 minutes later, 1 ml 4% thioglycolate broth or PBS were injected i.p. Animals were sacrificed 90 minutes later and the peritoneal fluid was harvested and centrifuged to remove blood cells before fluorescence was determined.

To determine extravasation in heart, 100  $\mu\text{l}$  of 2 mg/ml FITC-dextran or TRITC-dextran (40 or 10 kDa respectively) were i.v. injected. The animals were sacrificed 90 minutes later and the heart was flushed with PBS. The tissue was homogenized, centrifuged and the fluorescence was determined.

### Statistical Analysis

The results are presented as mean and SEM. SigmaPlot 12.5 (Systat Software) was used for statistical analysis. Unpaired two-tailed Student's t-test was used for comparisons of two groups (most of the presented experiments). Significance between more than two groups was tested by Two Way ANOVA using Holm-Sidak method as post-hoc test. The log-rank test was used to compare survival of mouse cohorts (Fig. 8B).  $p < 0.05$  was considered as statistically significant.

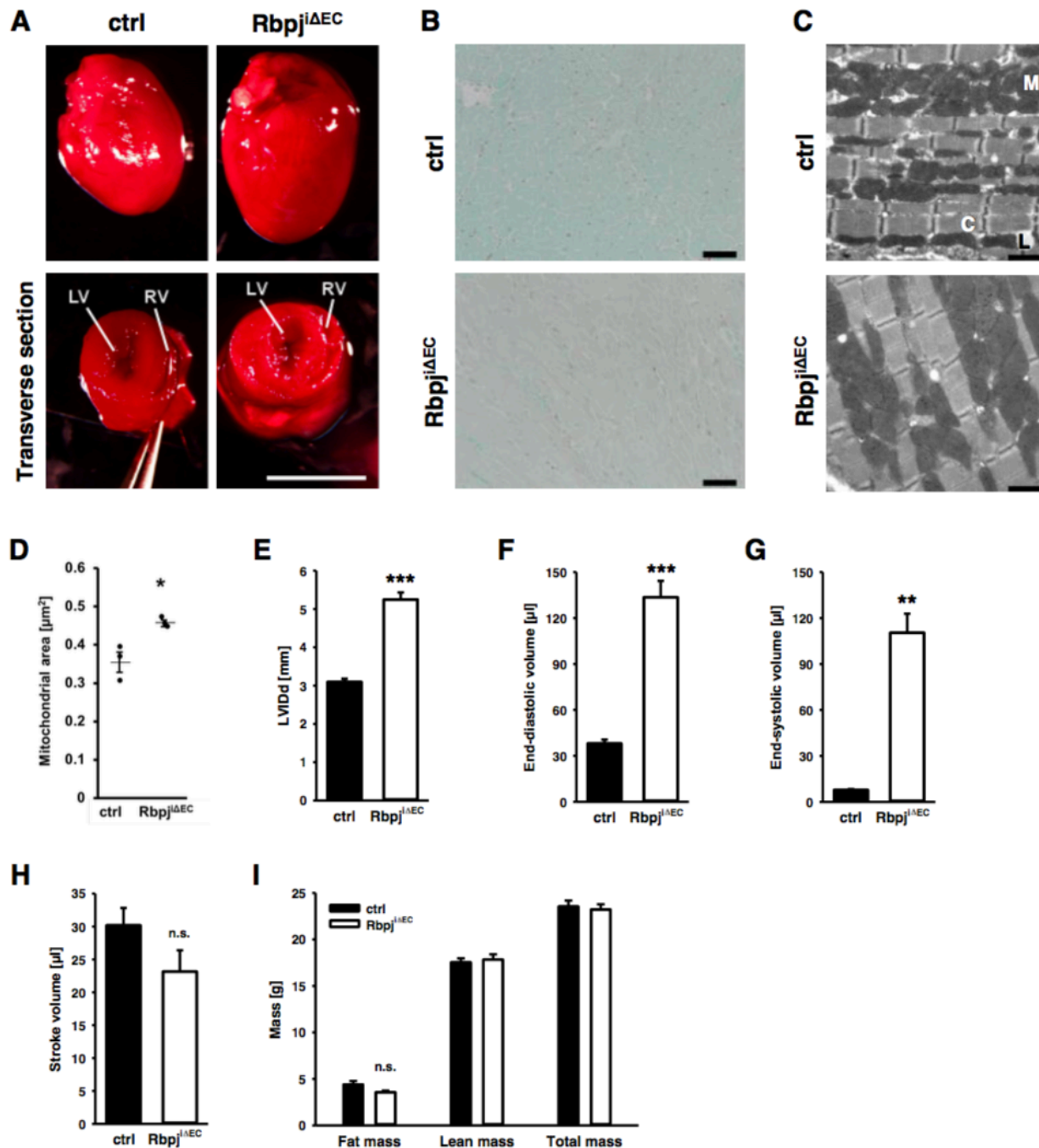
## Supplementary Figure 1



**Endothelial-specific ablation of Rbp-jκ in adult mice.** (A) Rbp-jκ protein expression in freshly isolated microvascular brain, lung and cardiac endothelial cells from control and *Rbpj*<sup>ΔEC</sup> mice

(pooled samples of 4 animals). **(B)** Rbp-j $\kappa$  protein detected in whole tissue lysates of heart, gastrocnemius muscle, liver and white adipose tissue (WAT). **(C)** Relative heart mass of control and *Rbpj*<sup>i $\Delta$ EC</sup> mice (n=4) 5 weeks after gene recombination. **(D-K)** Transthoracic echocardiography to determine stroke volume, ejection fraction, fractional shortening, left ventricle inner diameter during diastole (LVIDd) and systole (LVIDs), end diastolic volume and end-systolic volume of controls and *Rbpj*<sup>i $\Delta$ EC</sup> mice 4-5 weeks after gene recombination. Representative images of the transthoracic echocardiograms. Results are shown as mean and SEM; n=4 mice. **(L)** Representative image of surface electrocardiogram of control and *Rbpj*<sup>i $\Delta$ EC</sup> mice 6 weeks after gene recombination (n=3 mice per genotype analyzed).

## Supplementary Figure 2

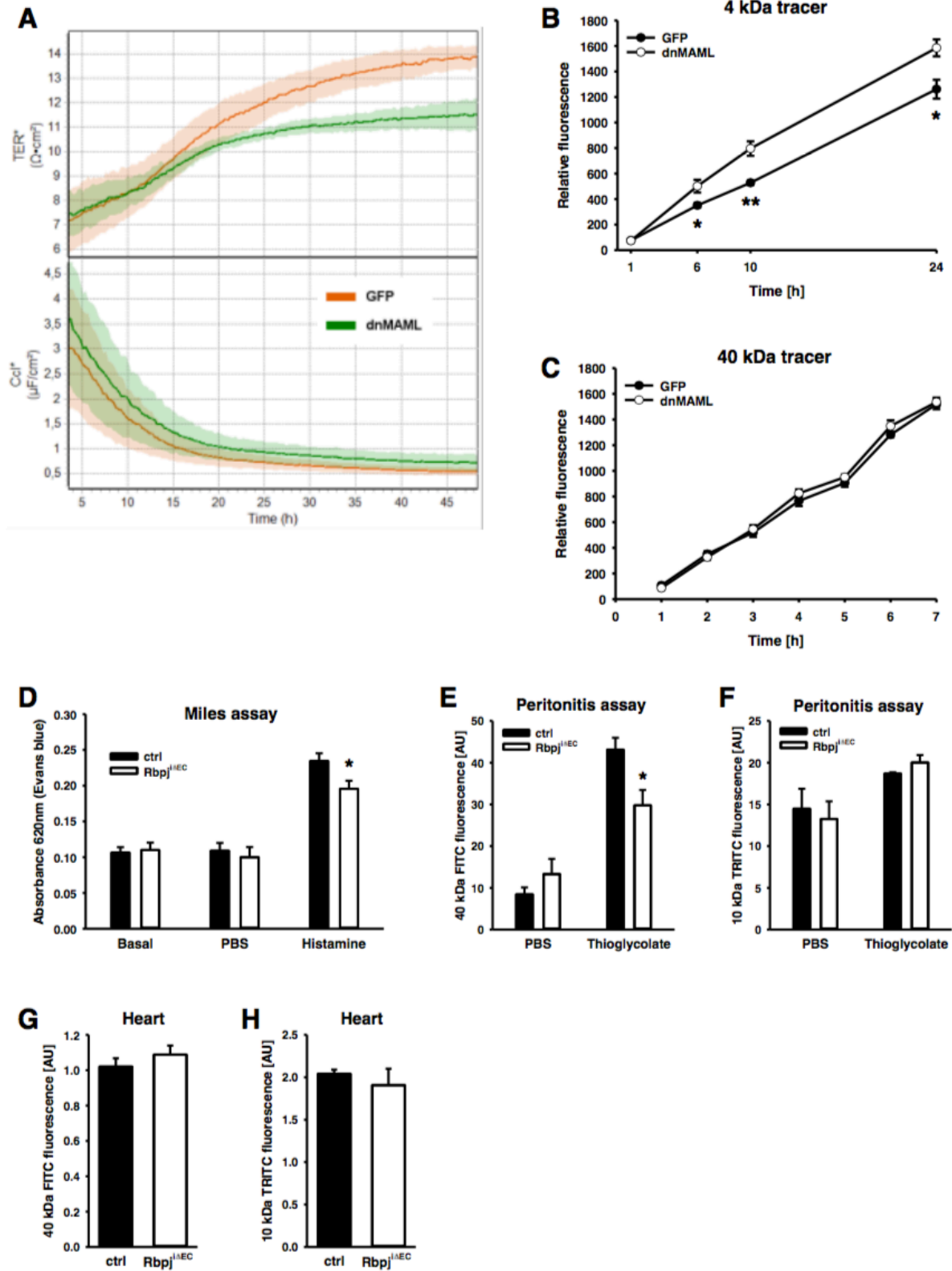


### Endothelial-specific *Rbpj* deletion impairs heart function.

(A) Hearts from control and *Rbpj*<sup>iΔEC</sup> mice seven weeks after gene recombination (LV, left ventricle; RV, right ventricle). (B) Trichrome staining showing no sign of fibrosis (blue color) in *Rbpj*<sup>iΔEC</sup> hearts seven weeks after gene recombination. (C, D) Electron micrographs of heart sections 8 weeks after gene inactivation (L, lipid droplet; C cardiac muscle; M, mitochondrion)

and quantification of mitochondrial area. **(E – H)** Left ventricle inner diameter during diastole (LVIDD), end-diastolic and end-systolic volume and stroke volume measured 8 weeks after recombination (n=5 mice). **(I)** Body mass, lean mass and fat mass of *Rbpj*<sup>iΔEC</sup> mice measured by EchoMRI (n=9 control and 11 *Rbpj*<sup>iΔEC</sup> mice) 8 weeks after recombination. Results are shown as mean and SEM, scale bar 5 mm (A), 50 μm (B), 1 μm (C). \*p<0.05; \*\*p<0.01; \*\*\*p<0.001; n.s. not significant.

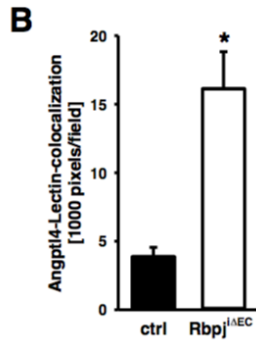
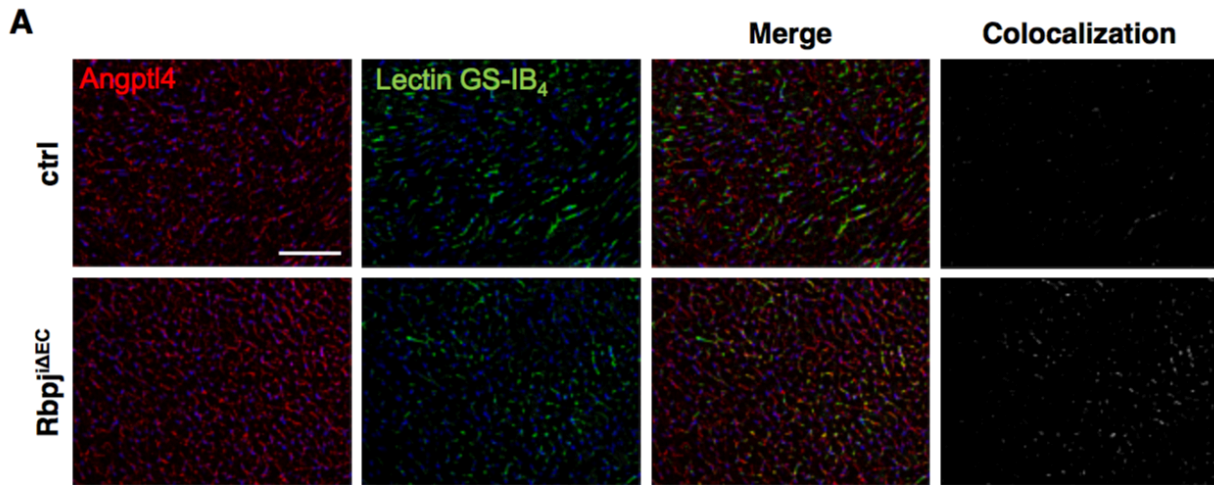
Supplementary Figure 3



**Loss of Notch signaling increases permeability of endothelial *in vitro* but not *in vivo*.**

(**A**) Transendothelial resistance and capacity of HUVEC transduced with GFP or dnMAML (representative chart). (**B, C**) Permeability of a HUVEC monolayer for 4 kDa and 40 kDa tracers upon Notch inhibition (n=4). (**D**) Dermal permeability for Evans Blue determined by Miles Assay (n≥8 mice). (**E – H**) Permeability for 40 kDa and 10kDa tracers determined by thioglycolate-induced peritonitis (90 minutes after thioglycolate injection) or in heart (n=3-5 mice). Results are shown as mean and SEM. \*p<0.05, \*\*p<0.01.

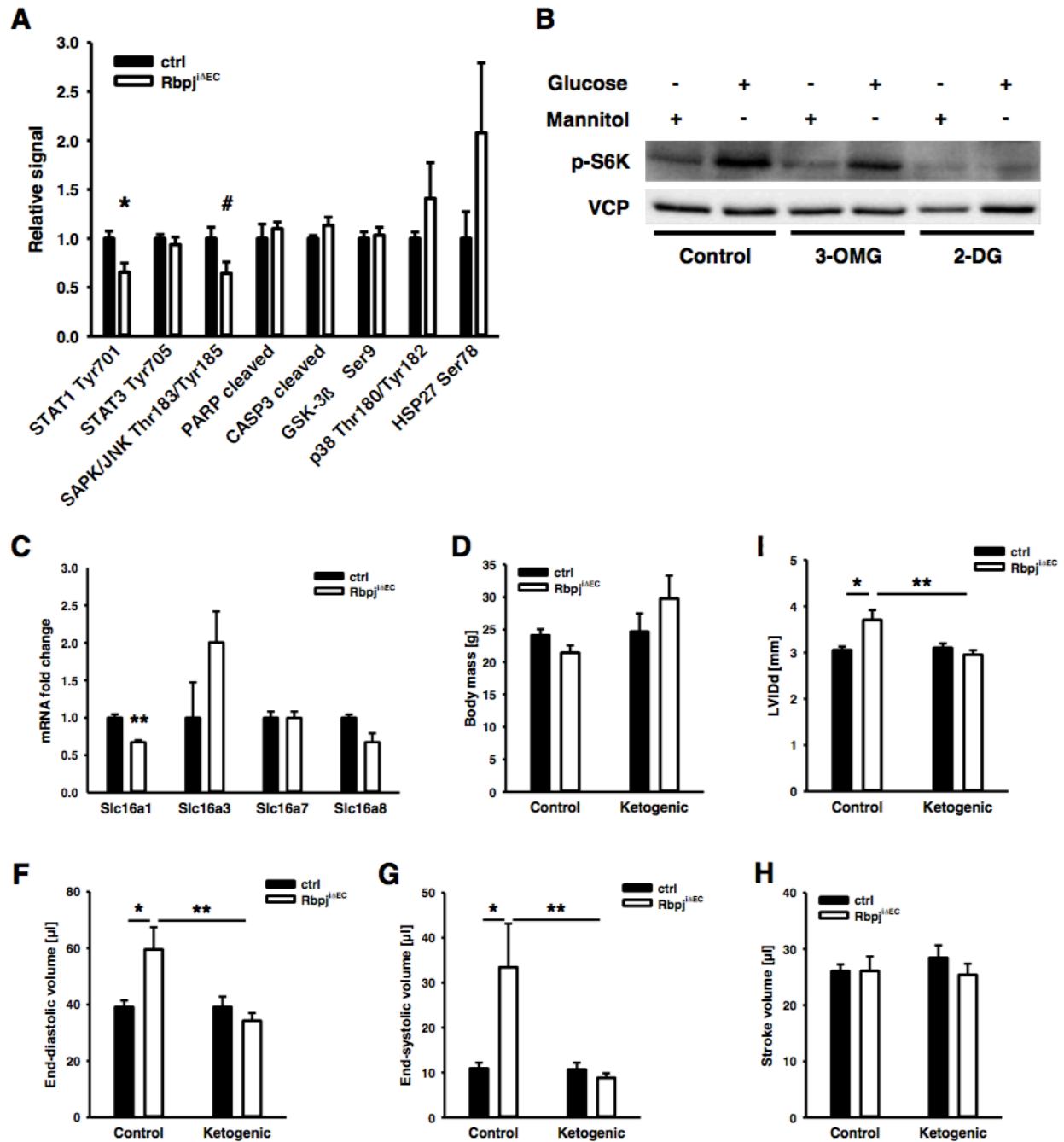
## Supplementary Figure 4



### Endothelial-specific *Rbpj* deletion improves *Angptl4* expression on the endothelium.

(A) Colocalization of *Angptl4* and endothelial cells stained with GS-IB<sub>4</sub>-lectin on heart sections of controls and *Rbpj*<sup>ΔEC</sup> mice. (B) Quantification. (n=3 hearts) 10 frames were analyzed per heart with ImageJ. Mean and SEM or representative pictures shown, scale bar 100 μm, \*p<0.05.

## Supplementary Figure 5



### Ketogenic diet prolongs survival upon endothelial *Rbpj* deletion.

(A) Additional results of an antibody array detecting specifically phosphorylated / activated proteins in lysates (n=4 hearts). (B) Western blot of primary neonatal rat cardiomyocytes treated with 5 g/l glucose or equimolar concentrations of mannitol, 3-O-methyl-glucose (3-OMG) or 2-deoxy-glucose (2-DG) detecting phosphorylated S6K and VCP (valosin containing

protein). (C) Expression of monocarboxylate transporters in heart lysates from control and *Rbpj*<sup>ΔEC</sup> mice (n=4). (D – H) Body mass and transthoracic echocardiography of mice kept on control or ketogenic diet (as indicated in Figure 8) (LVIDd, left ventricle diameter during diastole). Results are shown as mean and SEM, \*p<0.05, \*\*p<0.01, #p=0.12.

### Supplemental References

1. Ramasamy SK, Kusumbe AP, Wang L, Adams RH. Endothelial Notch activity promotes angiogenesis and osteogenesis in bone. *Nature*. 2014;507:376-380. doi:10.1038/nature13146.
2. Lehmann LH, Rostovsky JS, Buss SJ, Kreusser MM, Krebs J, Mier W, Enseleit F, Spiger K, Hardt SE, Wieland T, Haass M, Luscher TF, Schneider MD, Parlato R, Grone HJ, Haberkorn U, Yanagisawa M, Katus HA, Backs J. Essential role of sympathetic endothelin A receptors for adverse cardiac remodeling. *Proc Natl Acad Sci U S A*. 2014;111:13499-13504. doi:10.1073/pnas.1409026111.
3. Liebner S, Gerhardt H, Wolburg H. Differential expression of endothelial beta-catenin and plakoglobin during development and maturation of the blood-brain and blood-retina barrier in the chicken. *Dev Dyn*. 2000;217:86-98. doi:10.1002/(SICI)1097-0177(200001)217:1<86::AID-DVDY8>3.0.CO;2-E.
4. Brutsch R, Liebler SS, Wustehube J, Bartol A, Herberich SE, Adam MG, Telzerow A, Augustin HG, Fischer A. Integrin cytoplasmic domain-associated protein-1 attenuates sprouting angiogenesis. *Circ Res*. 2010;107:592-601. doi:10.1161/CIRCRESAHA.110.217257.
5. Woltje K, Jabs M, Fischer A. Serum induces transcription of Hey1 and Hey2 genes by Alk1 but not Notch signaling in endothelial cells. *PLoS One*. 2015;10:e0120547. doi:10.1371/journal.pone.0120547.
6. Furler SM, Cooney GJ, Hegarty BD, Lim-Fraser MY, Kraegen EW, Oakes ND. Local factors modulate tissue-specific NEFA utilization: assessment in rats using 3H-(R)-2-bromopalmitate. *Diabetes*. 2000;49:1427-1433.

### Supplementary Movie.

Transthoracic echocardiography 8 weeks after endothelial-specific *Rbpj* deletion.